WOODHEAD PUBLISHING SERIES IN CIVIL AND STRUCTURAL ENGINEERING

SEISMIC EVALUATION, DAMAGE, AND MITIGATION IN STRUCTURES

Edited by
IMAN MANSOURI
PAUL O. AWOYERA

ELSEVIER

Contents

List of contributors **xiii**
About the editors **xvii**
Preface **xix**

Part 1 Introduction to earthquake-induced damage evaluation and repairs in structures **1**

1 Damage indexes for performance assessment of low-rise reinforced concrete walls **3**
Julian Carrillo, Orlando Arroyo, and Sergio M. Alcocer
1.1 Introduction 3
1.2 Performance variables 4
1.2.1 Damage index based on residual cracking 4
1.2.2 Damage index based on a fractal dimension of cracking 6
1.2.3 Damage index based on stiffness degradation 9
1.2.4 Damage index based on the Park and Ang approach 13
1.3 Final remarks 15
Acknowledgments 15
References 15

2 Controlling the deflection of long steel beams using pretensioned cables **17**
Nader Fanaie and Fatemeh Partovi
Notations 17
2.1 Introduction 17
2.2 The pretensioned symmetric I-shaped steel beams with steel cables 20
2.3 The increment of the pretensioning force in the cable under external loading 21
2.3.1 The beam with simple supports and the V-shaped cable pattern 21
2.3.2 The beam with simple supports and the modified V-shaped cable pattern 22
2.3.3 The beam with simple supports and two V-shaped cable patterns 24

2.3.4 The beam with fixed supports and the V-shaped cable pattern 26
2.3.5 The beam with fixed supports and the modified V-shaped cable pattern 27
2.3.6 The beam with fixed supports and two V-shaped cable patterns 29
2.3.7 The cantilever beam along with the cables 30
2.4 Deflection 31
2.4.1 Maximum deflection of the beam with simple supports and the V-shaped cable pattern 32
2.4.2 Maximum deflection of the beam with simple supports and the modified V-shaped cable pattern 33
2.4.3 Maximum deflection of the beam with simple supports and two V-shaped cable patterns 34
2.4.4 Maximum deflection of the beam with fixed supports and the V-shaped cable pattern 34
2.4.5 Maximum deflection of the beam with fixed supports and the modified V-shaped cable pattern 35
2.4.6 Maximum deflection of the beam with fixed supports and two V-shaped cable patterns 36
2.4.7 Maximum deflection of cantilever beam along with cables 37
2.5 Finite element modeling of I-shaped symmetric pretensioned steel beams with steel cables 38
2.6 Calibration of theoretical relations with numerical models 41
2.7 The effects of horizontal cable length on the maximum deflections of the beams with simple and fixed supports with the modified V-shaped cable pattern 43
2.8 The effects of length a on the maximum deflections of the beams with simple and fixed supports with two V-shaped cable patterns 44
2.9 Comparison of bending moment diagrams of beams with and without cables 45
2.9.1 Comparison of bending moment diagrams of simply supported beams without cables and with cables 46
2.9.2 The comparison of the bending moment diagrams of the beams with fixed supports, with and without cables 46
2.9.3 The comparison of the diagrams of the bending moments of cantilever beams with and without cables 47
2.10 Conclusion 47
References 49

3 Cable-cylinder bracing system: theoretical background, structural behavior, and seismic design coefficients 51
Nader Fanaie and Ebrahim Afsar Dizaj
3.1 Introduction 51
3.2 Theoretical equilibrium relationships 53

3.3 Influence of cylinder size on behavior of the cable-cylinder bracing system 58
3.3.1 Cylinder length 58
3.3.2 Cylinder diameter 60
3.4 Influence of prestressing force of cables on the behavior of the cable-cylinder bracing system 61
3.5 Finite element modeling and validation 64
3.5.1 Verification of theoretical relationships 64
3.5.2 Influence of rigidity of the cylinder 65
3.6 Nonlinear time-history analysis 65
3.6.1 Case-study structures 65
3.6.2 Ground motions 69
3.6.3 Results and discussion 69
3.7 Proposed fiber element modeling technique and validation 72
3.8 Nonlinear dynamic analysis 78
3.9 Response modification factor 79
3.10 Influence of structural details on response modification factor 80
3.11 Sensitivity analysis 83
3.12 Proposing an equation for the response modification factor of cable-cylinder bracing system 93
3.13 Conclusion 94
References 95

4 Method of seismic resistance design—case studies 99
Jiulin Bai, Shuangshuang Jin, and Huiming Chen
4.1 Introduction 99
4.2 Method of seismic resistant design: reinforced concrete moment frames 99
4.2.1 Overview of the design approaches of reinforced concrete frames 99
4.2.2 Improved performance-based plastic design method for reinforced concrete moment frames 100
4.2.3 Code-based damage control design 108
4.3 Method of seismic resistance design: buckling-restrained brace-RCF systems 113
4.3.1 Buckling-restrained braces 114
4.3.2 Buckling-restrained brace-to-frame connection 117
4.3.3 Dual structural system for buckling-restrained brace-RCFs 119
4.3.4 Performance-based plastic design of buckling-restrained brace-RCF systems 119
4.3.5 Assessing and quantifying seismic performance of buckling-restrained brace-RCFs 122
4.3.6 Optimal seismic resistance design parameters 126
4.4 Method of seismic resistance design: steel plate shear wall-RCF systems 129

4.4.1 Overview of the dual structural system for steel plate shear wall-RCFs 129
4.4.2 PBPD method for steel plate shear wall-RC moment frames 130
4.4.3 Design examples 134
4.4.4 Assessing and quantifying seismic performance of steel plate shear wall-RCFs 135
4.5 Conclusion 138
References 139

5 Probabilistic seismic analysis of reinforced concrete frames using artificial intelligence-enhanced mechanical model 143
Huan Luo and Stephanie German Paal
5.1 Introduction 143
5.2 Methodology 145
5.2.1 Monte Carlo-based artificial intelligence-enhanced shear building model 145
5.3 Illustrative example 147
5.3.1 Description of selected building 148
5.3.2 Numerical results 149
5.4 Conclusion 153
References 154

6 Novel technique of performance-based optimum deign of buckling-restrained braced frames: colliding bodies optimization algorithms 157
B. Nouhi, F. Rezazadeh, S.M. Saraee, and Talatahari
6.1 Introduction 157
6.2 Buckling-restrained braced frames 158
6.3 Utilized algorithms 159
6.3.1 The standard colliding bodies optimization algorithm 160
6.3.2 The CBO2 algorithm (two-dimensional colliding bodies optimization) 162
6.3.3 The CBO3 algorithm (enhanced colliding bodies optimization) 163
6.3.4 The CBO4 algorithm (opposition-based colliding bodies optimization) 163
6.4 Structural analysis 165
6.5 Problem formulation 166
6.5.1 Objective function 166
6.5.2 Design constraints 167
6.6 Evaluation of the colliding bodies optimization algorithms 168
6.7 Design examples 168
6.7.1 Results 174
6.7.2 Layout optimization 178

6.8 Conclusion 181
References 181

7 Development and application of the Bouc–Wen model in seismic performance evaluation of reinforced concrete members 185
Shuo Wang, Xiaohui Yu, and Chao-Lie Ning
7.1 Introduction 185
7.2 Development of the Bouc–Wen model 186
7.3 Parameter identification 188
7.3.1 Columns 189
7.3.2 Joints 192
7.3.3 Walls 192
7.4 Seismic demand prediction using the Bouc–Wen model 194
7.5 Conclusion 197
References 199

Part 2 Repair of structural and non-structural components 203

8 Developing seismic fragility curves for caisson-type quay walls with improved backfill soil 205
Babak Ebrahimian and Amir Reza Zarnousheh Farahani
Symbols 205
8.1 Introduction 206
8.2 Numerical modeling 208
8.2.1 Constitutive model 208
8.2.2 Construction of the finite difference mesh 211
8.2.3 Boundary conditions 211
8.2.4 Interface characteristics 214
8.2.5 Damping characteristics 214
8.3 Validation of the developed numerical model 214
8.4 Improvement patterns of backfill soil behind caisson-type quay wall 215
8.5 Fragility analysis 215
8.5.1 Selection and preparation of input earthquake motions 215
8.5.2 Defining damage state criteria 219
8.5.3 Developing fragility curves 220
8.6 Comparing the effectiveness of various backfill improvement patterns of the caisson-type quay walls 222
8.7 Comparing the efficiencies of various backfill improvement patterns of the caisson-type quay walls 226
8.8 Summary and conclusions 229
Acknowledgments 230
References 231

Part 3 Seismic damage mitigation strategies 235

9 Machine learning approach for seismic assessment 237
Monique Head and Wael Aloqaily
9.1 Machine learning: an overview 237
9.2 Basic applications of machine learning 238
9.3 Examples of machine learning for seismic assessment 239
9.3.1 Response prediction 239
9.3.2 System identification and damage detection 240
9.3.3 Fragility curves and collapse capacity 240
9.3.4 Hazard analysis 240
9.4 Case study using neural networks for predicting earthquake responses 241
9.5 Challenges and future opportunities for machine learning and seismic assessment 243
References 244

10 Robust design of intelligent control systems to mitigate earthquake-induced vibrations under uncertain conditions 249
Javier Fernando Jiménez-Alonso, José M. Soria, Iván M. Díaz, and Andrés Sáez
10.1 Introduction 249
10.2 Tuned mass damper−shear building interaction model under earthquake action 252
10.3 Motion-based design method under uncertain conditions 256
10.4 Application example 261
10.4.1 Description of the benchmark building and preliminary analysis of its structural behavior 262
10.4.2 Motion-based design of the benchmark building equipped with active tuned mass damper under uncertain conditions 264
10.4.3 Motion-based design of the benchmark building equipped with semiactive tuned mass damper under uncertain conditions 265
10.4.4 Motion-based design of the benchmark building equipped with passive tuned mass damper under uncertain conditions 269
10.4.5 Discussion of the results 271
10.5 Conclusion 275
Acknowledgments 276
Declaration of conflicting interests 276
References 276

11 Multistory buildings equipped with innovative structural seismic shear fuse systems 279
Alireza Farzampour, Seyed Javad Mortazavi, Iman Mansouri, Paul O. Awoyera, and Jong Wan Hu
11.1 Introduction 279

11.2 Verification of modeling methodology 281
11.2.1 Finite element modeling methodology verification with laboratory test II 282
11.2.2 Validation of reduced order models implemented for multistory structures modeling and conventional systems 284
11.3 Dampers equipped with butterfly-shaped link design procedure 285
11.3.1 Brittle and ductile limit states for dampers equipped with butterfly-shaped shear links 286
11.3.2 Controlling the drift ratios and stiffness equation requirement 289
11.4 Design of prototype six-story structure with structural shear links 291
11.4.1 The comparison of the monotonically loaded butterfly-shaped damper system with conventional EBF system 293
11.5 Discussion of the results for nonlinear response history analysis for multistory building 293
11.6 Nonlinear response history analysis results under for butterfly-shaped and conventional EBF systems 297
11.7 Conclusion 302
Statements and declarations 302
Funding 302
Competing interests 303
Data availability 303
References 303

12 Seismic protection strategies for damage mitigation in structures 307
Ayşegül Erdoğan, Süleyman İpek, and Esra M. Güneyisi
Abbreviations 307
12.1 Introduction 307
12.2 Seismic protection strategies 310
12.2.1 Seismic isolation systems 310
12.2.2 Passive energy dissipation systems 317
12.2.3 Semiactive and active systems 327
12.2.4 Hybrid systems 331
12.3 Conclusions 333
References 333

13 Analytical formulas of the mechanical behavior of rubber bearings considering the isolator nonlinearities and the influence of shear modulus 343
Konstantinos N. Kalfas and Davide Forcellini
13.1 Introduction 343
13.2 Validation of the numerical models and sensitivity analysis 345
13.2.1 Mechanical properties and validation of rubber bearings 345
13.2.2 Design of the numerical models 348

13.2.3 Numerical analyses and boundary conditions 349
13.3 Mechanical behavior of rubber bearings 350
13.3.1 Analytical, linear elastic model 350
13.3.2 Development of the nonlinear rubber bearing model 352
13.3.3 Analytical formula accounting for the nonlinear relationship between G_b, θ, and P 353
13.3.4 Influence of the behavior of rubber bearings from the shear modulus, G_b 358
13.4 Conclusion 359
References 360

14 Mitigation of deformations of a hunchbacked block-type gravity quay wall subjected to dynamic loading through optimizing its back-face configuration 365
Babak Ebrahimian and Amir Reza Zarnousheh Farahani
14.1 Introduction 365
14.2 Numerical simulation of the seismic behavior of hunchbacked block-type gravity quay wall 367
14.3 Sensitivity analysis on hunch angle, backfill friction angle, and hunch height-to-wall height ratio 371
14.4 Estimation of the optimum hunch angle corresponding to the minimum deformation of the wall 374
14.5 Summary and conclusions 377
References 378

15 Model-based adaptive control system for magneto-rheological damper-controlled structures 381
Zubair Rashid Wani
15.1 Introduction 381
15.2 Methodology 382
15.2.1 Basic principle of response-based adaptive control 382
15.3 Control strategy formulation 383
15.3.1 Design and modeling of the controlled structure 383
15.3.2 Implementation of control algorithm 383
15.4 Numerical study 386
15.4.1 Control parameters of magneto-rheological dampers 387
15.4.2 Optimizing the number of controllers 391
15.5 Results and discussions 391
15.6 Conclusion 396
References 397

Index 399

Cable-cylinder bracing system: theoretical background, structural behavior, and seismic design coefficients

3

Nader Fanaie[1] *and Ebrahim Afsar Dizaj*[2]
[1]Department of Civil Engineering, K. N. Toosi University of Technology, Tehran, Iran,
[2]Department of Civil Engineering, Azarbaijan Shahid Madani University, Tabriz, Iran

3.1 Introduction

Lateral load-resisting systems are recognized as an efficient approach to mitigating the excessive damage of structures under earthquake loading [1]. Bracing systems have been among the most popular lateral systems for structural engineers. Several researchers have used different bracing configurations to enhance the lateral stiffness and ductility of existing steel frames [2,3]. Among the typical bracing systems, implementing the most recent types of bracing systems, called buckling restrained braces, as well as novel dampers, to improve the seismic response of buildings, was investigated in several studies [4−10].

Over the past decades, several studies have investigated the advantages of using cable bracing system as an advanced tool to control the excessive lateral displacement of existing steel moment-resisting frames under seismic shaking [11]. The research in this area, however, was not limited to steel frames. Several pieces of research have focused on applying cables in reinforced concrete beams as an alternative to conventional shear reinforcement.

In literature, cables are known as axial tensile load-resisting members with negligible flexural rigidity. Cables are frequently used in large-span roofs and bridges [12−16]. Due to their advantages, researchers have studied the application of cable bracing in existing structures. In tall buildings, cables are used to keep the lateral displacement of the structure in its allowable limit state [11]. Some studies have investigated the application of cables in preventing the progressive damage of steel frames [17,18] and bridges [19]. Recently, different types of cable bracing systems have been proposed by various researchers [20−23]. Cables as bracing systems have several advantages, such as (1) high capacity in tolerating tensile forces, (2) high flexibility, (3) easy and fast installation and construction, and (4) causing fewer noises during installation [21].

Cable-cylinder bracing system, proposed by Tagawa and Hou [24] for strengthening of steel moment-resisting frames, is a novel configuration of cable bracing

Seismic Evaluation, Damage, and Mitigation in Structures. DOI: https://doi.org/10.1016/B978-0-323-88530-0.00014-3

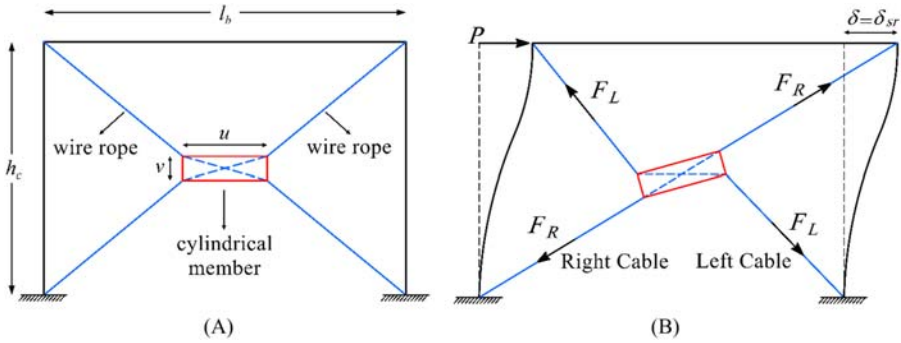

Figure 3.1 Cable-cylinder bracing system: (A) configuration and (B) deformed shape [26].

systems. In this system, the cables and hollow cylinder are used together in such a way that the wire ropes pass at their intersections. Fig. 3.1 shows a typical configuration of a cable-cylinder bracing system. Both the PVC and steel pipes, with either high or low flexural rigidity, can be used as the cylinder. In Fig. 3.1A l_b is the length of the beam, h_c is the height of columns, u is the cylinder length, and v is the inner diameter of the cylinder. The rotation of the cylinder, as it is shown in Fig. 3.1B, causes both the cables to be in tension up to the $\delta = \delta_{sr}$, where δ_{sr} is the lateral displacement of the frame corresponding to the straightening of one of the cables. In Fig. 3.1B, F_L and F_R are the axial tensile forces of the left and right cables, respectively, corresponding to the δ. The structural behavior of the cable-cylinder bracing system, however, depends significantly on the flexural rigidity, the prestressing force of the cables, and cylinder dimension [25].

Currently, strengthening the existing moment-resisting steel frames using X cables is a common practice of structural engineers. Replacing the X cables with cable-cylinder bracing could have several advantages, as summarized below:

1. The cable-cylinder bracing system has negligible lateral stiffness at low drift ratios. Therefore adding this system to the moment frames will not affect the fundamental period of a structure [27].
2. The cable-cylinder bracing system can effectively prevent the damage concentration in a specific building story; therefore it prevents the formation of the soft story in a building frame [27].
3. The cable-cylinder bracing system can act as a passive control system to prevent the excessive lateral drift of the existing structure without increasing the base shear or causing an increase in the compressive axial load of columns.

The study presented herein aims to comprehensively investigate the structural performance of the cable-cylinder bracing system as a promising alternative to the conventional X cable bracing system. To this end, the theoretical background of this system and its governing equilibrium relationships are presented. Subsequently, the effect of cylinder dimension and the level of prestressing force on the behavior of this system are discussed. Then, the nonlinear static and dynamic responses of this bracing system are compared with those of the conventional cable bracing

system. Using the incremental dynamic analysis (IDA) results, the response modification factor of this system is estimated. Finally, a sensitivity analysis is carried out on this system, and an equation is proposed for the *R* factor (response modification factor) of the proposed cable-cylinder bracing system.

In the following sections, the above items are presented in detail.

3.2 Theoretical equilibrium relationships

Fig. 3.2A shows the configuration and deformed shape of a simple frame braced with the cable-cylinder bracing system. In this figure, all the parameters involved in the derivation of theoretical equations are shown. Here, for simplicity, the cylinder is supposed to be rigid. Pushing the frame δ mm toward the right (where under this displacement, the behavior of the frame is in the elastic range), the center point of the cylinder (O) will move as $\delta/2$ mm and will rotate as θ radians toward the counterclockwise direction (Fig. 3.2B). It should be noted that it is assumed that the center point of the cylinder will not move alongside the vertical axis. Using the equilibrium laws for the cylinder, the relationships between δ and θ are derivated. Subsequently, the variation of lateral static loading (P) against δ (i.e., P-δ curve), as well as the variation of the strain of cables (ε) versus δ (i.e., ε-δ curve), is plotted.

Assuming that the cylinder is placed in the center of the frame, the slope of the cable AE will be equal to that of cable GC. Similarly, the slope of cables BF and HD will be the same. From Fig. 3.2B, under δ displacement of the frame toward the right, the coordinate of points A, B, C, and D will be $\begin{bmatrix}0\\0\end{bmatrix}$, $\begin{bmatrix}\delta\\h_c\end{bmatrix}$, $\begin{bmatrix}l_b+\delta\\h_c\end{bmatrix}$ and $\begin{bmatrix}l_b\\0\end{bmatrix}$, respectively. Therefore the updated coordinates of the cylinder boundaries and center points, that is, points E, F, G, H, and O will be

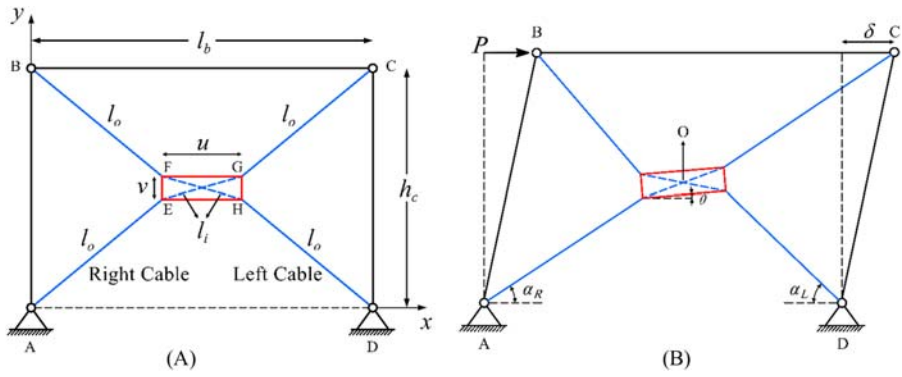

Figure 3.2 Important points and dimensions involved in the derivation of theoretical equations: (A) undeformed state and (B) deformed state.

$\frac{1}{2}\begin{bmatrix}(l_b+\delta)-u\cos\theta+v\sin\theta\\ h_c-u\sin\theta-v\cos\theta\end{bmatrix}$, $\begin{bmatrix}(l_b+\delta)-u\cos\theta-v\sin\theta\\ h_c-u\sin\theta+v\cos\theta\end{bmatrix}$, $\frac{1}{2}\begin{bmatrix}(l_b+\delta)+u\cos\theta-v\sin\theta\\ h_c+u\sin\theta+v\cos\theta\end{bmatrix}$, $\frac{1}{2}\begin{bmatrix}(l_b+\delta)+u\cos\theta+v\sin\theta\\ h_c+u\sin\theta-v\cos\theta\end{bmatrix}$, and $\frac{1}{2}\begin{bmatrix}l_b+\delta\\ h_c\end{bmatrix}$, respectively.

From the equilibrium law, the summation of moments about O should be zero $\left(\left(\sum M_o=0\right)\right)$; therefore:

$$\mathrm{F_R}\times\frac{\left|\vec{AE}\times\vec{EG}\right|}{\left|\vec{AE}\right|}=F_L\times\frac{\left|\vec{DH}\times\vec{FH}\right|}{\left|\vec{DH}\right|} \tag{3.1}$$

where F_L and F_R can be obtained from Eqs. (3.2−3.3):

$$F_L=\frac{AE}{L_{DH}+L_{Ho}}\times\Delta_{DH} \tag{3.2}$$

$$F_R=\frac{AE}{L_{AE}+L_{EO}}\times\Delta_{AE} \tag{3.3}$$

where E and A are the modulus of elasticity and cross-sectional area of each cable, Δ_{AE} is the elongation of cable AE and Δ_{DH} is the elongation of cable DH. Therefore Eq. (3.1) can be rewritten as:

$$\Delta_{AE}\times\frac{\left|\vec{AE}\times\vec{EG}\right|}{\left|\vec{AE}\right|}=\Delta_{DH}\times\frac{\left|\vec{DH}\times\vec{FH}\right|}{\left|\vec{DH}\right|} \tag{3.4}$$

Eq. (3.4) is expressed considering the undeformed (initial) length of the cables, cross product of direction of each cable, and elongation of cables. The coordinate of vectors AE, EG, FH, and DH will be $\frac{1}{2}\begin{bmatrix}(l_b+\delta)-u\cos\theta+v\sin\theta\\ h_c-u\sin\theta-v\cos\theta\end{bmatrix}$, $\begin{bmatrix}u\cos\theta-v\sin\theta\\ u\sin\theta+v\cos\theta\end{bmatrix}$, $\begin{bmatrix}u\cos\theta+v\sin\theta\\ u\sin\theta-v\cos\theta\end{bmatrix}$, and $\frac{1}{2}\begin{bmatrix}(l_b-\delta)-u\cos\theta-v\sin\theta\\ -h_c-u\sin\theta+v\cos\theta\end{bmatrix}$, respectively. Having these coordinates, the cross products presented in Eq. (3.4) can be obtained from Eqs. (3.5−3.6):

$$\left|\vec{AE}\times\vec{EG}\right|=\frac{1}{2}\left|(l_b+\delta)(u\sin\theta+v\cos\theta)-h_c(u\cos\theta-v\sin\theta)\right| \tag{3.5}$$

$$\left|\vec{DH}\times\vec{FH}\right|=\frac{1}{2}\left|(l_b-\delta)(u\sin\theta-v\cos\theta)+h_c(u\cos\theta+v\sin\theta)\right| \tag{3.6}$$

Therefore Δ_{AE} and Δ_{DH} can be determined using Eqs. (3.7−3.8), respectively:

$$\Delta_{AE}=\frac{1}{2}\sqrt{((l_b+\delta)-u\cos\theta+v\sin\theta)^2+(h_c-u\sin\theta-v\cos\theta)^2}-\frac{1}{2}\sqrt{(l_b-u)^2+(h_c-v)^2} \tag{3.7}$$

$$\Delta_{DH} = \frac{1}{2}\sqrt{((l_b-\delta)-u\cos\theta-v\sin\theta)^2+(-h_c-u\sin\theta+v\cos\theta)^2} - \frac{1}{2}\sqrt{(l_b-u)^2+(h_c-v)^2} \tag{3.8}$$

Putting Eqs. (3.5–3.8) into Eq. (3.4) will lead to the following implicit Eq. (3.9) which relates cylinder rotation to the lateral static displacement of the frame:

$$\begin{aligned}\left[1-\frac{\sqrt{(l_b-u)^2+(h_c-v)^2}}{\sqrt{((l_b+\delta)-u\cos\theta+v\sin\theta)^2+(h_c-u\sin\theta-v\cos\theta)^2}}\right] \\ \times\left|(l_b+\delta)(u\sin\theta+v\cos\theta)-h_c(u\cos\theta-v\sin\theta)\right| \\ =\left[1-\frac{\sqrt{(l_b-u)^2+(h_c-v)^2}}{\sqrt{((-l_b+\delta)+u\cos\theta+v\sin\theta)^2+(h_c+u\sin\theta-v\cos\theta)^2}}\right] \\ \times\left|(-l_b+\delta)(-u\sin\theta+v\cos\theta)+h_c(u\cos\theta+v\sin\theta)\right|\end{aligned} \tag{3.9}$$

The angles α_L and α_R (shown in Fig. 3.2) can be expressed as follows:

$$\cos\alpha_R = \cos\alpha_{\overrightarrow{AE}} = \frac{(l_b+\delta)-u\cos\theta+v\sin\theta}{\sqrt{((l_b+\delta)-u\cos\theta+v\sin\theta)^2+(h_c-u\sin\theta-v\cos\theta)^2}} \tag{3.10}$$

$$-\cos\alpha_L = \cos\alpha_{\overrightarrow{DH}} = -\frac{(-l_b+\delta)+u\cos\theta+v\sin\theta}{\sqrt{((-l_b+\delta)+u\cos\theta+v\sin\theta)^2+(h_c+u\sin\theta-v\cos\theta)^2}} \tag{3.11}$$

From the equilibrium equation, the summation of horizontal forces should be zero $\left(\sum F_x = 0\right)$.This will lead to the following relationship between P and δ:

$$P = \frac{2AE}{l_t}\left[\begin{array}{l}\Delta_{AE}\times\dfrac{(l_b+\delta)-u\cos\theta+v\sin\theta}{\sqrt{((l_b+\delta)-u\cos\theta+v\sin\theta)^2+(h_c-u\sin\theta-v\cos\theta)^2}} \\ +\Delta_{DH}\times\dfrac{(-l_b+\delta)+u\cos\theta+v\sin\theta}{\sqrt{((-l_b+\delta)+u\cos\theta+v\sin\theta)^2+(h_c+u\sin\theta-v\cos\theta)^2}}\end{array}\right] \tag{3.12}$$

where l_t is the total length of each cable ($l_t = l_i + 2l_o$) as shown in Fig. 3.2. In Fig. 3.2 l_o is the length of each cable outside the cylinder and l_i is the length of the cable inside the cylinder.

Eqs. (3.13−3.14) present the relationship between the strain of right cable (ε_R) and the strain of left cable (ε_L) with δ:

$$\varepsilon_R = \frac{1}{2}\left[\frac{\sqrt{((l_b+\delta)-u\cos\theta+v\sin\theta)^2+(h_c-u\sin\theta-v\cos\theta)^2}-\frac{1}{2}\sqrt{(l_b-u)^2+(h_c-v)^2}}{L_{AE}+L_{Eo}}\right] \tag{3.13}$$

$$\varepsilon_L = \frac{1}{2}\left[\frac{\sqrt{((l_b-\delta)-u\cos\theta-v\sin\theta)^2+(-h_c-u\sin\theta+v\cos\theta)^2}-\frac{1}{2}\sqrt{(l_b-u)^2+(h_c-v)^2}}{L_{DH}+L_{Ho}}\right] \tag{3.14}$$

It is worth noting that the above equations are valid until a cable straightened. Once one of the cables straightened, the other cable will not tolerate axial force anymore, because the summation of moments about O should be zero (equilibrium equation). Beyond this, the slopes of the cables inside and outside of the cylinder will be equal for the straightened cable. Moreover, the other cable will be loosened. Considering the deformed shape of the frame shown in Fig. 3.2B, for $\delta > \delta_{sr}$ the elongation of cable AC will be equal to $\delta\cos\theta$ ($\delta_{AC} = \delta\cos\theta$). Therefore the strain of cable AC (ε_{AC}) can be expressed in term of δ using Eq. (3.15):

$$\varepsilon_{AC} = \frac{\delta_{AC}}{l_{AC}} = \delta\frac{l_b}{{l_b}^2+{h_c}^2} \tag{3.15}$$

Moreover, from the equilibrium equation, the lateral force of the storey (P) can be related to the δ using Eq. (3.16):

$$P = AE\frac{l_b}{{l_b}^2+{h_c}^2}\delta\times\frac{l_b}{\sqrt{{l_b}^2+{h_c}^2}} = \frac{{l_b}^2}{\left({l_b}^2+{h_c}^2\right)^{\frac{3}{2}}}AE\delta \tag{3.16}$$

Using Eq. (3.16), in Fig. 3.3 the variation of the P/AE is plotted against δ. To plot Fig. 3.3, as a numerical example, it is assumed that $l_b = 4$ m, $h_c = 3$ m, $u = 22$ cm, and $v = 5$ cm. For comparison, the same curve is also plotted for the X cable bracing system.

Fig. 3.3 shows that the lateral stiffness of the cable-cylinder bracing system is approximately zero in the initial stages of the loading, but its value increases as the story displacement increases. This finding confirms that the cable-cylinder bracing system will not change the fundamental period of the frame. However, as can be seen in Fig. 3.3, the lateral stiffness of the X cable bracing system is a constant parameter and is significantly greater than that of the cable-cylinder bracing system.

Fig. 3.4 shows the strain variation of left and right cables versus the δ using Eqs. (3.13−3.14). In this figure, RC and LC denote the right and left cables, respectively.

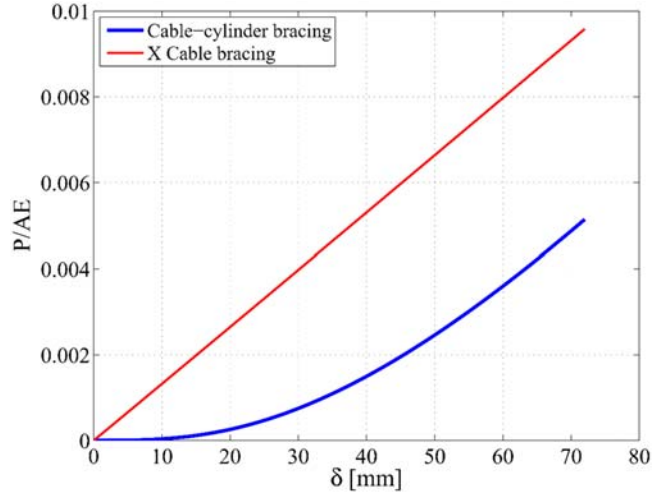

Figure 3.3 Comparing the variation of story force versus story displacement in cable-cylinder and X cable bracing systems.

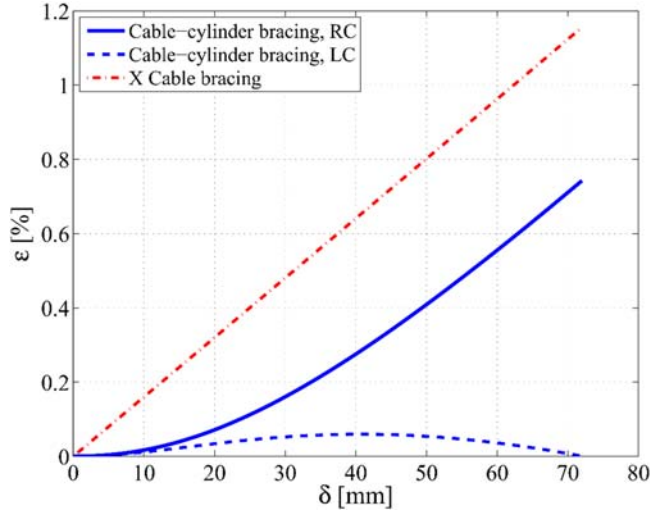

Figure 3.4 Comparing ε-δ curves of cable-cylinder and X cable bracing systems.

Fig. 3.4 shows that cables of the cable-cylinder bracing system will reach their fracture strain in higher story displacements. This will increase the ductility of the frame comparing to the X cable bracing system. Moreover, as Fig. 3.4 shows, both the cables are in tension in a wide storey displacement range in this bracing system. Therefore the impulses (caused by the loosening of cables) will be improved using the cable-cylinder bracing system. However, as discussed earlier in the text, once

the lateral story displacement reached the δ_{sr} (toward the right), the right cable will be straightened while the force will be zero in the left cable. Therefore, to ensure that both the left and right cables are in tension, the cylinder length and diameter should be selected such that δ_{sr} be equal or slightly greater than the target damage limit state (in terms of lateral displacement) of the frame. Moreover, the cylinder size should be selected to allow the cables to reach their fracture strain at the displacement limit of the frame.

The next section sheds light on the importance of cylinder size in the cable-cylinder bracing system.

3.3 Influence of cylinder size on behavior of the cable-cylinder bracing system

The cylinder size (both the length and diameter) is an important parameter affecting the structural behavior of the cable-cylinder bracing system. Such dimension of the cable should be selected that makes it to be crooked. The following equation shows the proportionality of the cable length (u) and diameter (v) with the beam length (l_b), and column height (h_c):

$$\frac{v}{u} < \frac{h_c}{l_b} \tag{3.17}$$

where u/v is the slope of the cable inside the cylinder and h_c/l_b is the slope of the cable in the corresponding X cable bracing system. The more the difference between the slopes of cables outside and inside the cylinder, the more the difference between the structural behavior of the cable-cylinder and the X cable bracing systems. Apparently, for $\frac{v}{u} = \frac{h_c}{l_b}$ the cable-cylinder bracing system will behave the same as the X cable bracing system.

3.3.1 Cylinder length

In this section, to study the impact of cylinder length on the structural behavior of a steel frame braced with the cable-cylinder bracing system, the results presented in Figs. 3.3 and 3.4 are reproduced for different cylinder lengths. To this end, various cylinder lengths (u) are considered, including 20, 22, 24, 26, and 28 cm. Other parameters are supposed to be the same as those considered to plot Figs. 3.3 and 3.4.

Fig. 3.5 shows P-δ curves and Fig. 3.6 shows ε-δ curves for the various considered cylinder lengths. The curves shown in these figures are plotted up to $\delta = \delta_{sr}$ (i.e., up to where one of the cables become straightened), where the value of δ_{sr} is different for each case. Figs. 3.5 and 3.6 indicates that as cylinder length increases, the value of δ_{sr} increases as well. Moreover, Fig. 3.5 shows that for a given δ the value of P/AE becomes lesser for the frame with the greater length of the cylinder, therefore as cylinder length increases, the frame can sustain larger lateral

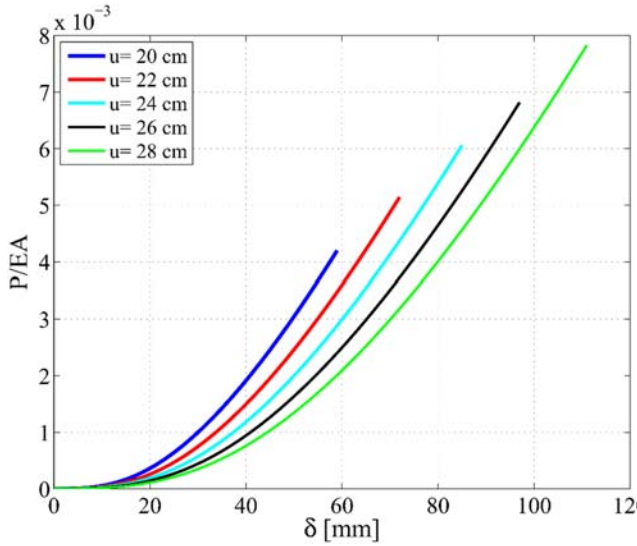

Figure 3.5 *P-δ* curves for the cable-cylinder braced frame with different cylinder lengths.

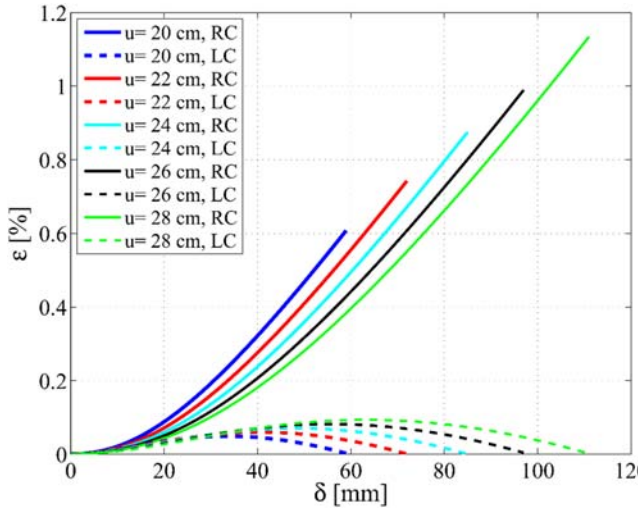

Figure 3.6 *ε-δ* curves for the cable-cylinder braced frame with different cylinder lengths.

displacement. This implies that the larger the cylinder length is, the higher ductility of the frame is. Fig. 3.6 shows that in a wider range both the cables are in tension, that is, the cables can sustain larger tensile strain to reach $\delta = \delta_{sr}$. The reason is behind the geometry of the braced frame shown in Fig. 3.2. For the larger cylinder

length, more rotation of the cable is needed to cause the cable to become straightened (i.e., to reach $\delta = \delta_{sr}$). Therefore, for the greater cylinder length, the frame should be pushed more to reach δ_{sr}.

In the next section, the influence of cylinder diameter on the structural performance of the cable-cylinder bracing system is discussed.

3.3.2 Cylinder diameter

Figs. 3.7 and 3.8 present the P-δ and ε-δ curves for different hypothetical cylinder diameters, respectively. Here, the internal cylinder diameter is considered to be 4, 5, 6, and 8 cm. Other variables are assumed to be the same as those considered to plot Figs. 3.3 and 3.4. Same as Figs. 3.5 and 3.6, in Figs. 3.7 and 3.8 the curves are plotted up to $\delta = \delta_{sr}$.

Fig. 3.7 shows that despite the cylinder length, an increase in the cylinder diameter results in a decrease in the value of δ_{sr}. For example, as can be seen in Fig. 3.7, while for 4 mm of cylinder diameter δ_{sr} is approximately 82 mm, for the same frame with 8 mm of cylinder diameter δ_{sr} is around 38 mm. Moreover, Fig. 3.8 shows that the greater the cylinder diameter is, the smaller the tensile strain corresponding to the δ_{sr} is. For example, while for the active cable with 4 mm cylinder diameter, the associated tensile strain of δ_{sr} is approximately 0.0088; for the same case with 8 mm cylinder diameter, the corresponding strain of active cable to δ_{sr} is 0.004. Therefore it can be concluded from the results presented in Figs. 3.7 and 3.8 that increasing the diameter of the cylinder has a negative influence on the ductility of the braced frame.

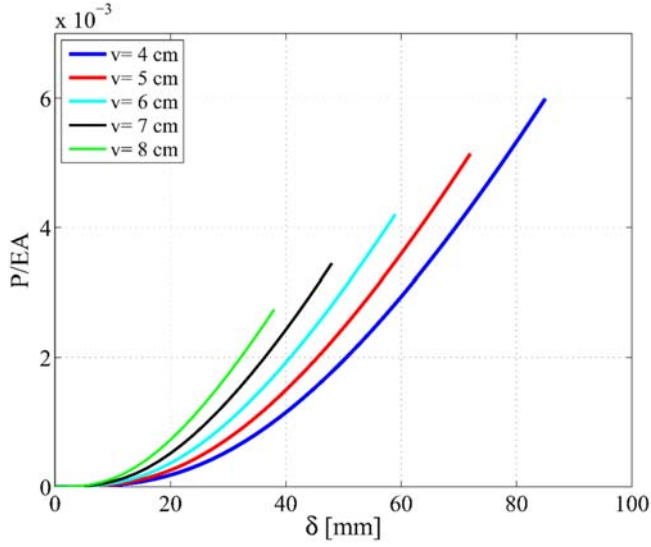

Figure 3.7 P-δ curves for the cable-cylinder braced frame with different cylinder diameters.

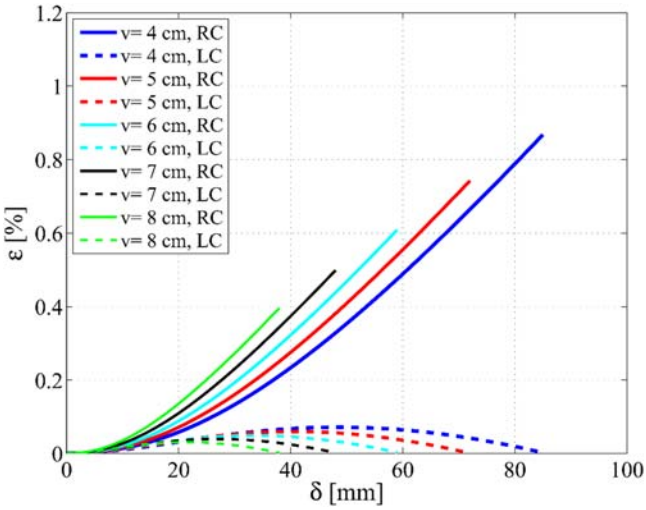

Figure 3.8 ε-δ curves for the cable-cylinder braced frame with different cylinder diameters.

3.4 Influence of prestressing force of cables on the behavior of the cable-cylinder bracing system

This section studies the effect of prestressing force of cables on the structural performance of the cable-cylinder bracing system. If the prestressing force in the cables is supposed to be F_p, the moment equilibrium of the cylinder can be expressed as Eq. (3.18):

$$\left(\frac{l_t}{2AE}F_P + \Delta_{AE}\right) \times \left|\frac{\vec{AE} \times \vec{EG}}{\vec{AE}}\right| = \left(\frac{l_t}{2AE}F_P + \Delta_{DH}\right) \times \left|\frac{\vec{DH} \times \vec{FH}}{\vec{DH}}\right| \tag{3.18}$$

Putting Eqs. (3.5−3.8) into Eq. (3.18), the following implicit relationship between θ, δ, and F_p will be obtained:

$$\begin{aligned}
&\left[\frac{l_t}{AE}F_P + \sqrt{((l_b+\delta)-u\cos\theta+v\sin\theta)^2 + (h_c-u\sin\theta-v\cos\theta)^2} - 2l_e\right] \\
&\qquad \times \frac{\left|(l_b+\delta)(u\sin\theta+v\cos\theta) - h_c(u\cos\theta-v\sin\theta)\right|}{\sqrt{((l_b+\delta)-u\cos\theta+v\sin\theta)^2 + (h_c-u\sin\theta-v\cos\theta)^2}} \\
&= \left[\frac{l_t}{AE}F_P + \sqrt{((-l_b+\delta)+u\cos\theta+v\sin\theta)^2 + (h_c+u\sin\theta-v\cos\theta)^2} - 2l_e\right] \\
&\qquad \times \frac{\left|(-l_b+\delta)(-u\sin\theta+v\cos\theta) + h_c(u\cos\theta+v\sin\theta)\right|}{\sqrt{((-l_b+\delta)+u\cos\theta+v\sin\theta)^2 + (h_c+u\sin\theta-v\cos\theta)^2}}
\end{aligned} \tag{3.19}$$

The equilibrium of the horizontal forces will yield Eq. (3.20):

$$P = F_R \cos\alpha_R - F_L \cos\alpha_L \tag{3.20}$$

where F_R and F_L are the axial force in the right and left cables, respectively (Eqs. 3.21–3.22):

$$F_R = \frac{2AE}{l_t}\left(\Delta_{AE} + \frac{F_p l_t}{2AE}\right) \tag{3.21}$$

$$F_L = \frac{2AE}{l_t}\left(\Delta_{DH} + \frac{F_p l_t}{2AE}\right) \tag{3.22}$$

Putting Eqs. (3.21–3.22) into Eq. (3.20) will give the following equation:

$$P = \frac{2AE}{l_t}\left[\begin{array}{l}\left(\Delta_{AE} + \frac{F_p l_t}{2AE}\right) \times \frac{(l_b+\delta) - u\cos\theta + v\sin\theta}{\sqrt{((l_b+\delta) - u\cos\theta + v\sin\theta)^2 + (h_c - u\sin\theta - v\cos\theta)^2}} \\ + \left(\Delta_{DH} + \frac{F_p l_t}{2AE}\right) \times \frac{(-l_b+\delta) + u\cos\theta + v\sin\theta}{\sqrt{((-l_b+\delta) + u\cos\theta + v\sin\theta)^2 + (h_c + u\sin\theta - v\cos\theta)^2}}\end{array}\right] \tag{3.23}$$

The tensile strain in right and left cables, therefore, can be expressed using the following equations:

$$\varepsilon_R = \frac{2\Delta_{AE}}{l_t} + \frac{F_p}{AE} \tag{3.24}$$

$$\varepsilon_L = \frac{2\Delta_{DH}}{l_t} + \frac{F_p}{AE} \tag{3.25}$$

Employing Eq. (3.23), in Fig. 3.9 the P-δ curves corresponding to various prestressing levels, including 0 (without prestressing), 200, 400, 600, and 800 MPa are shown. Other parameters are supposed to be the same as those assumed to plot Fig. 3.3.

Fig. 3.9 shows that as the prestressing level increases the value of δ_{sr} increases significantly. This means that the prestressing force causes both cables to be active in a wider range of lateral frame displacement. For example, the 800 MPa prestressing level of the cables increases the δ_{sr} from approximately 70 mm (for the case without prestressing) to around 100 mm. Therefore the prestressing force will increase the ductility of the frame.

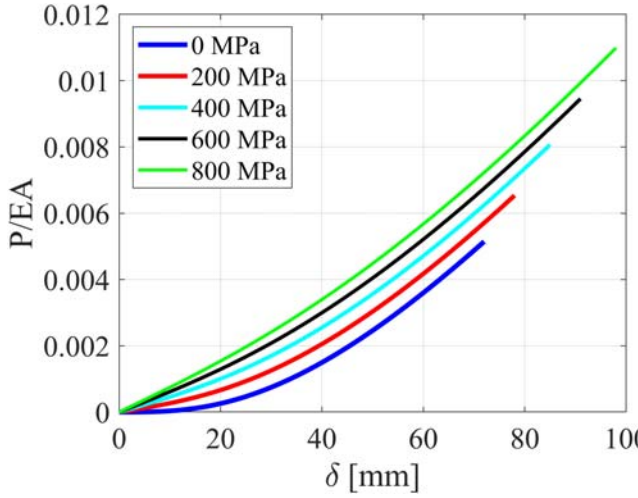

Figure 3.9 *P-δ* curves for the cable-cylinder braced frame with different prestressing levels.

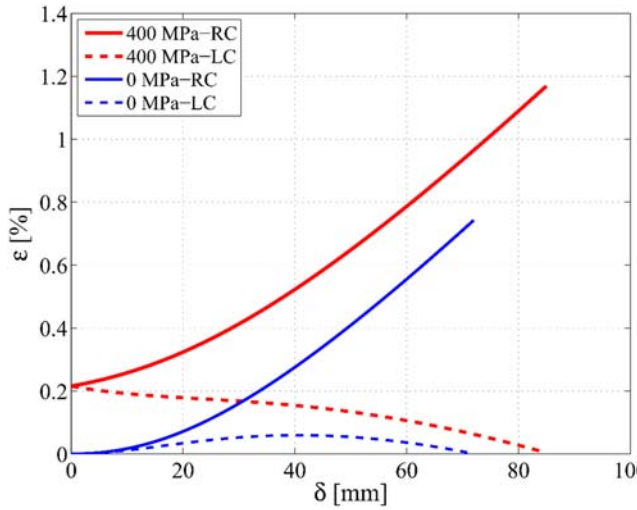

Figure 3.10 *ε-δ* curves for the cable-cylinder braced frame with different prestressing levels.

Fig. 3.10 shows the effect of prestressing level of the cables on *ε-δ* curves. To this end, the *ε-δ* curves of left and right cables without prestressing force are compared with those corresponding to the 400 MPa prestressing level of cables.

Fig. 3.10 indicates that the prestressing force of the cables causes them to tolerate higher tensile strains before the lateral displacement of the frame equals δ_{sr}. Therefore the cables will be active for the higher value of δ, and therefore the ductility of the frame will be increased significantly.

3.5 Finite element modeling and validation

3.5.1 Verification of theoretical relationships

In this section, the validity of the theoretical equations developed in the previous sections of the chapter is investigated using the finite element modeling technique. To this end, a portal frame with hinged beam-column connections braced with the cable-cylinder bracing system is simulated in the Abaqus finite element platform. The modeling is carried out in both the two-dimensional (2D) and 3D spaces. To simulate the frame, it is assumed that $l_b = 4$ m, $h_c = 3$ m, $u = 22$ cm, and $v = 5$ cm. For the columns, a $100 \times 100 \times 8$ mm box profile is considered and for the cables, the cross-sectional area is regarded as 1 cm^2. Moreover, the cylinder is assumed to be a rigid element.

In Fig. 3.11 P-δ curves and in Fig. 3.12 ε-δ curves of theoretical relationships are compared with those of 2D and 3D finite element models.

As can be seen in Fig. 3.11, there is a slight difference between the results of finite element models and the theoretical relationships. This is because the axial deformation of columns and beam was disregarded in the development of theoretical equations. Moreover, the contact between the cable and cylinder is modeled more realistically in the 3D model. However, in the 2D model, the cables outside and inside of the cylinder are simulated as separate truss elements.

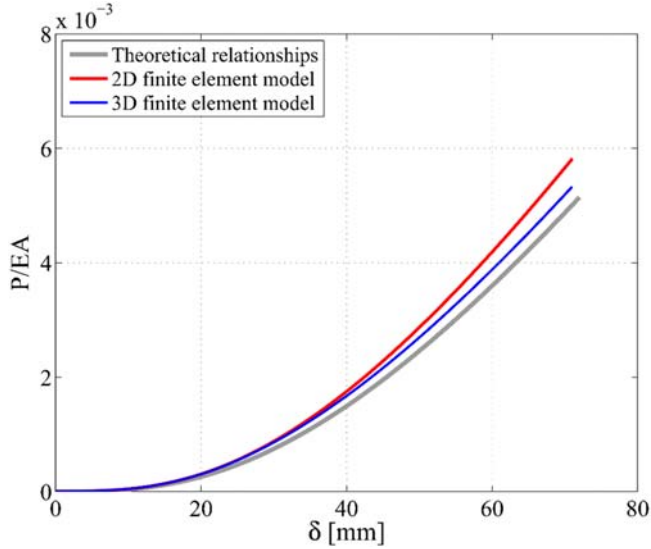

Figure 3.11 Comparing P-δ curves of theoretical relationships with those of finite element simulation.

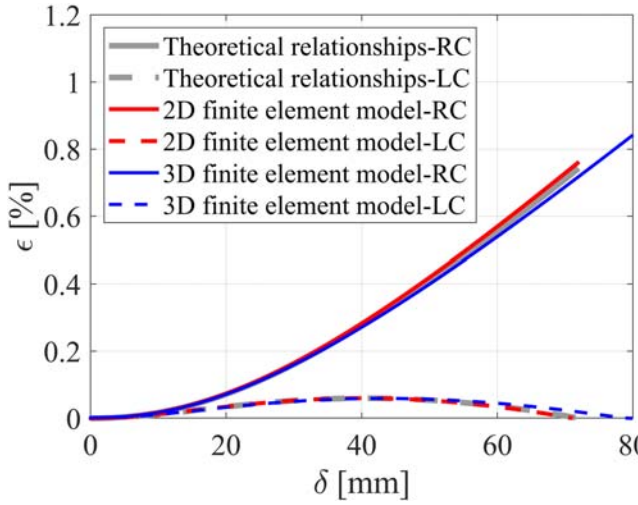

Figure 3.12 Comparing ε-δ curves of theoretical relationships with those of finite element simulation.

3.5.2 Influence of rigidity of the cylinder

To investigate the influence of rigidity of the cylinder on the structural performance of the cable-cylinder bracing system, two nonlinear pushover analyses carried out on the hypothetical frame employed in the previous section using the 3D modeling scheme. In the first analysis, the cylinder is considered to be fully rigid, and in the second analysis, the modulus of elasticity of the cylinder was taken as $0.001E_s$ (i.e., soft cylinder), where E_s is the modulus of elasticity of cables. The thickness of the cylinder was assumed to be 5 mm. Figs. 3.13 and 3.14 compare the P-δ and ε-δ curves of the cable-rigid cylinder system with those of the cable-soft cylinder system.

As Figs. 3.13 and 3.14 show, the results of the rigid and soft cylinders are approximately the same. As mentioned earlier in the text, in this study the theoretical equations are developed assuming the rigid cylinder, therefore this assumption will not affect the results significantly. Here, to perform nonlinear time-history analyses (NTHAs) (next section), the properties of the cylinder are considered to be the same as those of the cables.

3.6 Nonlinear time-history analysis

3.6.1 Case-study structures

In this study, three case-study structures including 2, 4, and 6-storey moment-resisting steel frames are considered to evaluate the dynamic response of the cable-cylinder bracing system. Two different strengthening methodologies are considered here for comparison: (1) using conventional X cable bracings and (2) using the

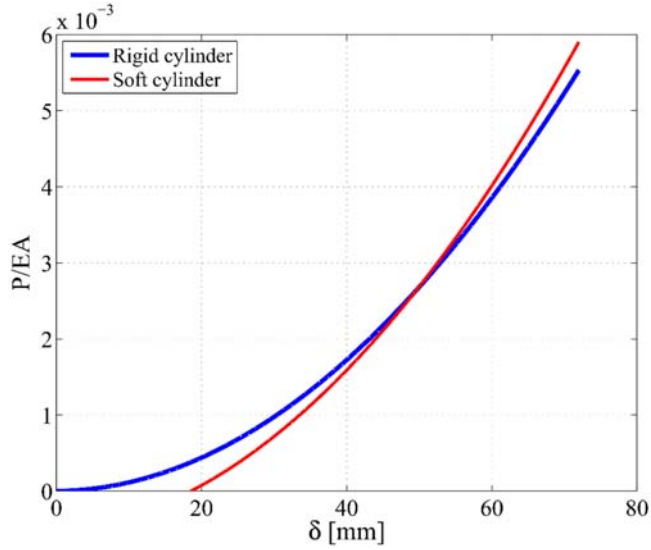

Figure 3.13 Influence of rigidity of the cylinder on *P*-δ curves of simple frame braced with the cable-cylinder bracing system.

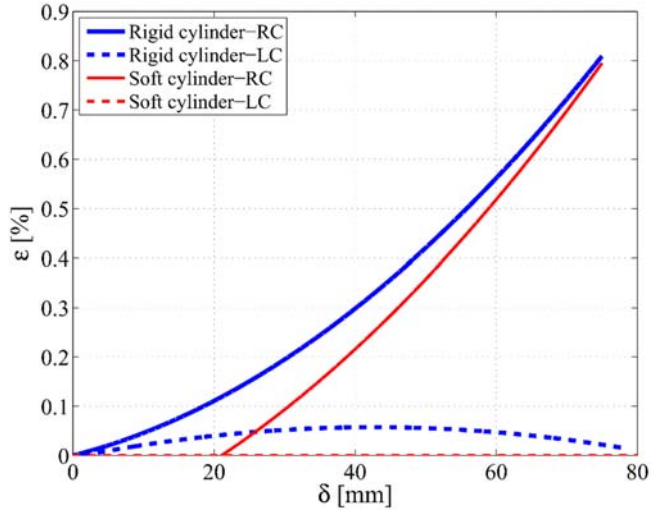

Figure 3.14 Influence of rigidity of the cylinder on ε-δ curves of simple frame braced with the cable-cylinder bracing system.

cable-cylinder bracing system. The plan and elevation view of the considered moment frames are shown in Fig. 3.15. As an example, the schematic view of the 4-story moment-resisting frame strengthened with X cable and the cable-cylinder bracing systems is shown in Fig. 3.16. These frames are designed based on the

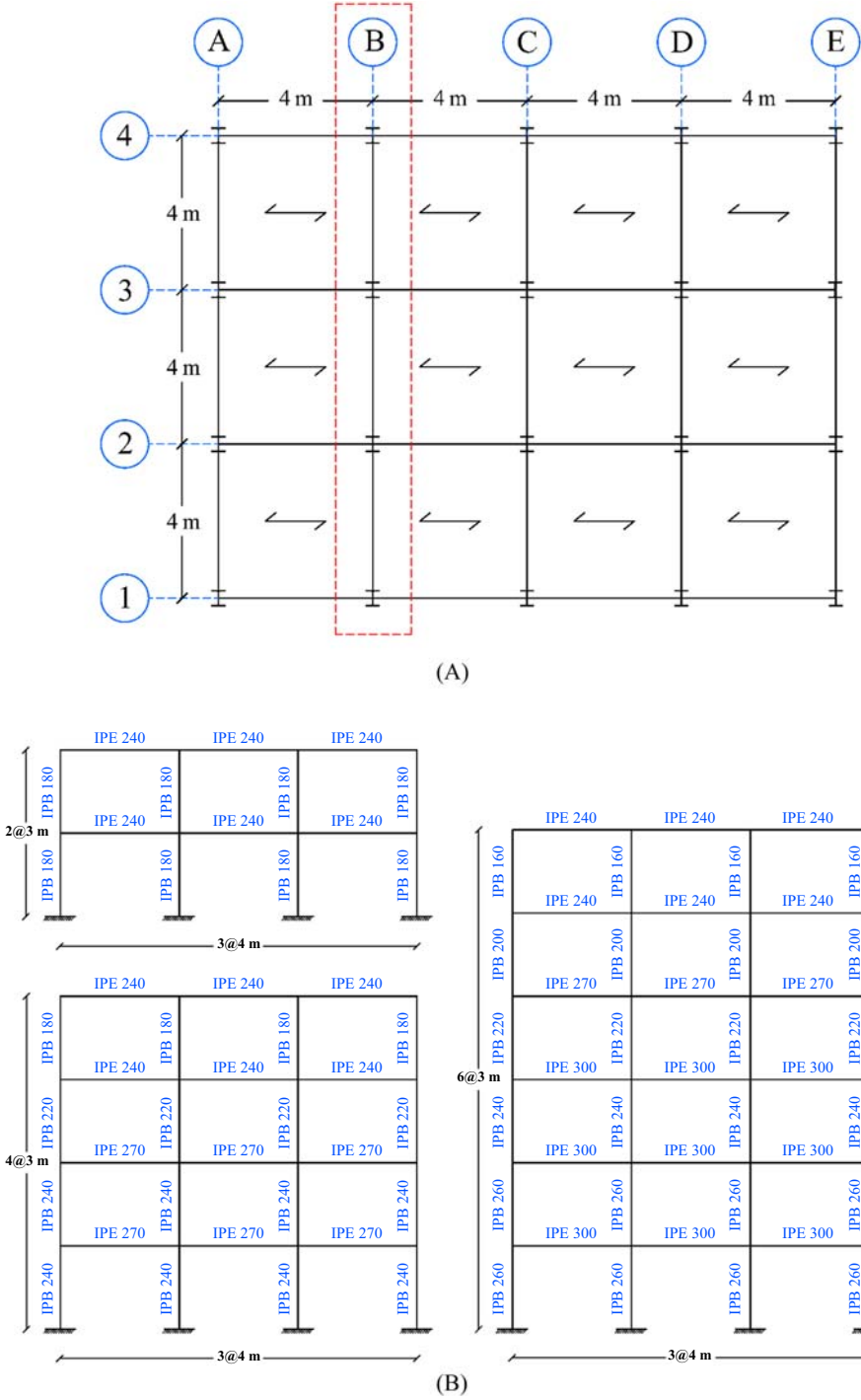

Figure 3.15 The studied moment-resisting frames: (A) plan view and (B) elevation view.

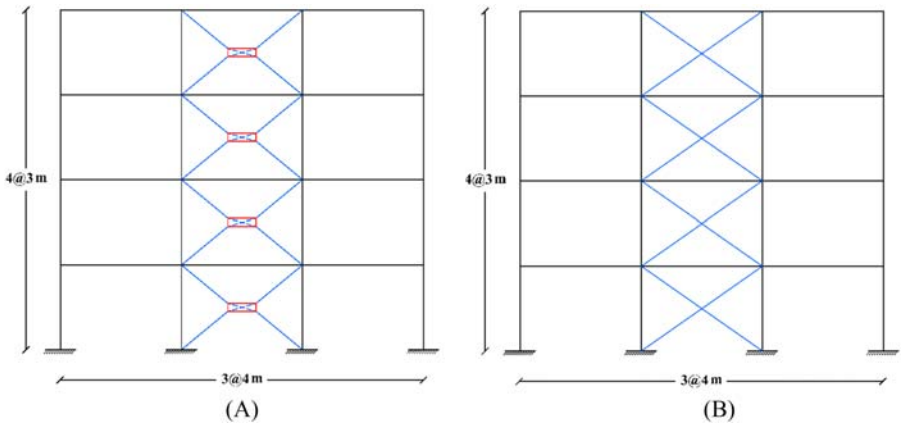

Figure 3.16 The considered strengthening systems: (A) cable-cylinder bracing system and (B) X cable bracing system.

Table 3.1 The natural periods of the case-study frames.

Number of storeys	Steel frame (s)	Steel frame braced with cable-cylinder bracings (s)	Steel frame braced with X cable bracings (s)
2	0.8	0.33	0.8
4	1.26	0.58	1.26
6	1.7	0.85	1.7

AISC360−10 [28] code. The considered frames are assumed to be located in Tehran. To design the frames, the live load and dead load on each story floor are assumed to be 2 and 6 kN/m^2, respectively. The seismic loading is calculated based on the specifications provided in ASCE7−10 [29]. All the story floors are considered to be rigid.

In order to conduct NTHA, for simplification, the 2D frame in B-axis (Fig. 3.15A) is extracted from the structure and simulated in Abaqus. The reason behind this simplification is to reduce the analyses time. The nonlinear elastoplastic material is adopted to simulate the nonlinear behavior of steel material used in beam and columns. A bilinear constitutive stress−strain model with yielding stress of 240 MPa (representing ST-37 steel grade) and a postyield strain hardening ratio of 0.02 is considered here. Rayleigh damping was used in dynamic analyses.

Based on the eigenvalue analysis, the natural period of the considered frames was evaluated and tabulated in Table 3.1. As can be seen in Table 3.1, the natural period of frames braced with X cable bracings is lower than that of corresponding moment-resisting frames. However, the natural period of frames braced with cable-cylinder bracings is the same as that of moment-resisting frames. This is because the cable-cylinder braces are not active in the lower lateral displacements due to their geometry.

3.6.2 Ground motions

To carry out the NTHA, five ground motions records of important earthquakes worldwide, including Morgan Hill, Loma Prieta, Northridge, Kobe, and Bam, were selected from the NGA database [30]. Fig. 3.17 shows the spectral acceleration spectrum of these ground motion records. The selected records scaled to PGA = 0.35 g, to comply with the Iranian code of practice for the seismic-resistant design of buildings, Standard No. 2800 [31], where the buildings located in high seismicity regions are designed for PGA = 0.35 g.

It is worth mentioning that the cross sectional-area of cables in X cable bracing system was calculated to remain within the elastic range under the ground motion records scaled to PGA = 0.350 g. The cross-sectional area of cables in the cable-cylinder bracing system was considered the same as those of the X cable bracing system. Using this procedure, the cross-sectional area of cables is considered to be 5.9, 6.5, and 7 cm^2 for 2-, 4-, and 6-story case-study frames, respectively.

3.6.3 Results and discussion

3.6.3.1 Hysteretic response

In this section, the hysteretic base shear−roof displacement response of the case-study structures under the Kobe ground motion record is discussed. Figs. 3.18−3.20 show the hysteretic response of the 2-, 4-, and 6-story frames, respectively. Fig. 3.18 shows that the moment-resisting frame tolerates relatively large lateral displacements; more specifically, large residual displacements can be seen in the

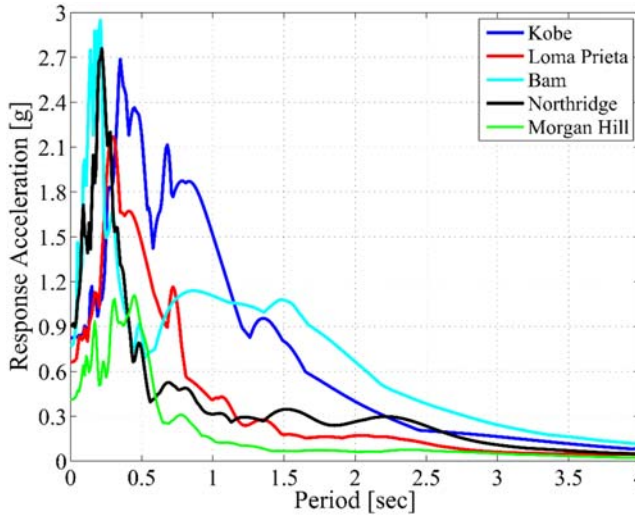

Figure 3.17 Spectral acceleration spectrum of the selected ground motions to conduct NTHAs. *NTHAs*, Nonlinear time-history analyses.

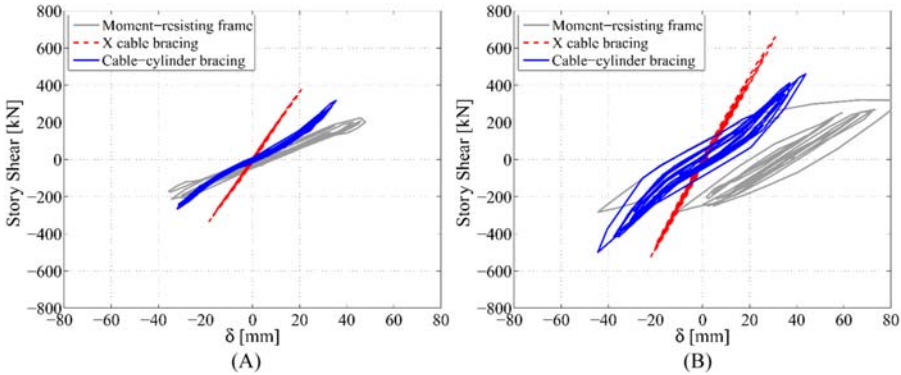

Figure 3.18 Comparing the hysteresis response of 2-story case-study frames: (A) story 2 and (B) story 1.

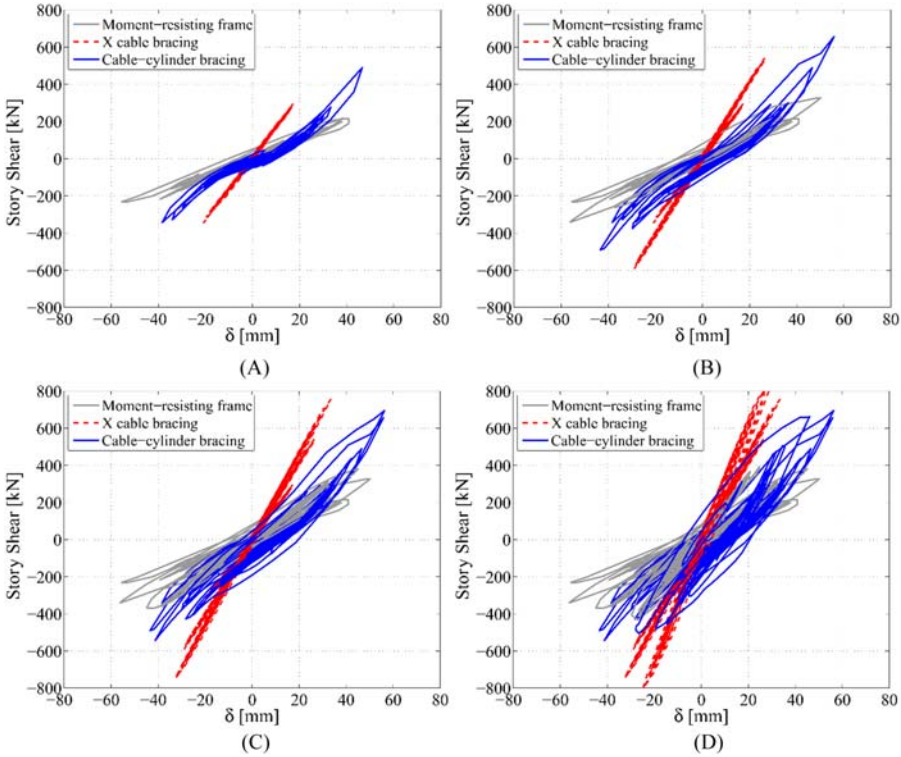

Figure 3.19 Comparing the hysteresis response of 4-story case-study frames: (A) story 4, (B) story 3, (C) story 2, and (D) story 1.

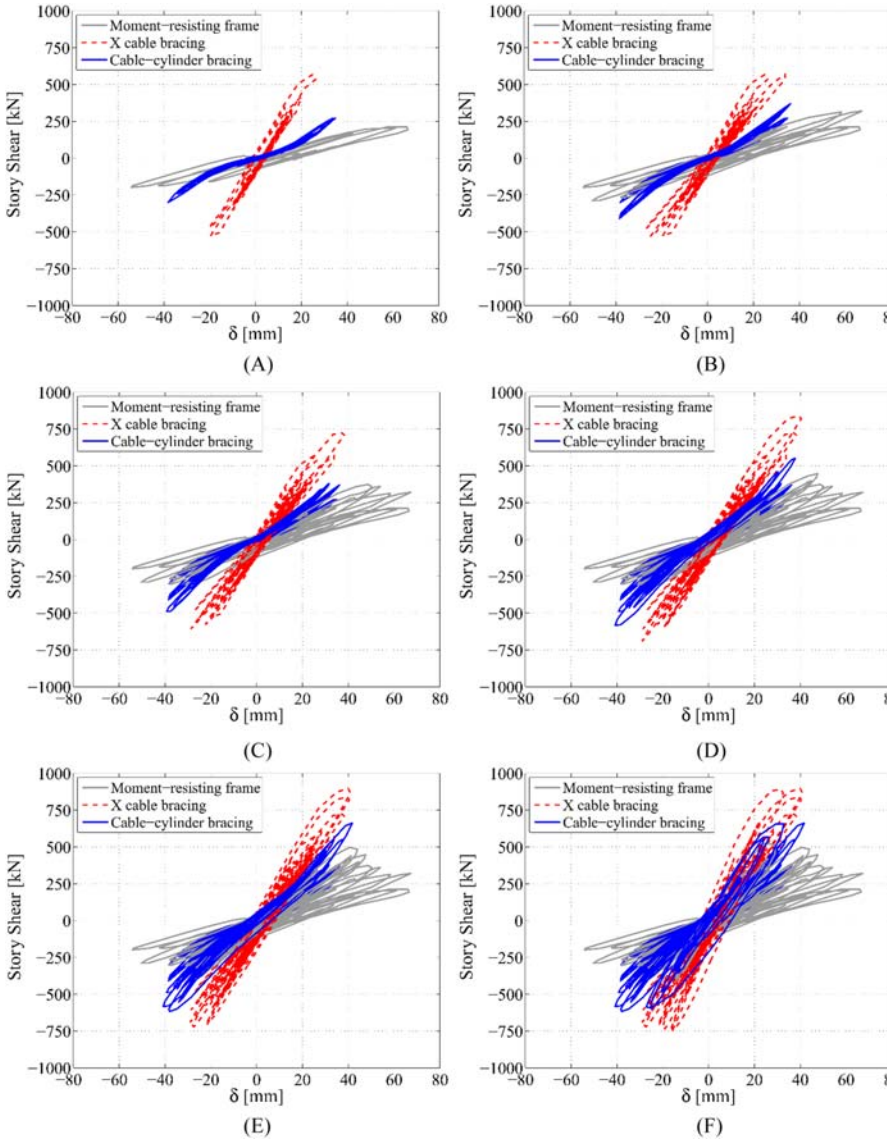

Figure 3.20 Comparing the hysteresis response of 6-story case-study frames: (A) story 6, (B) story 5, (C) story 4, (D) story 3, (E) story 2, and (F) story 1.

first story of this frame. However, adding X cables significantly reduces the lateral displacement, because this system significantly increases the lateral stiffness of the structure. However, this bracing system significantly increases the story shear in comparison with the cable-cylinder bracing system. This triggers higher axial forces in the cables, which applies higher axial compressive forces to the adjacent column.

Fig. 3.19 shows that in the lower story levels, the area under the base shear−lateral displacement response of the frame braced with the cable-cylinder bracing system is considerably higher than the moment-resisting frame and frame braced with X cable bracing system. This confirms the advantage of the cable-cylinder bracing system in comparison with the X cable bracing system. The results presented in Fig. 3.20 are in line with those presented in Figs. 3.18 and 3.19). Therefore it can be concluded that the able-cylinder bracing system is an effective tool for improving the seismic performance of moment-resisting steel frames.

3.6.3.2 Distribution of drifts along with the height of structures

Figs. 3.21−3.23 show the distribution of the drift ratio along with the height of the case-study structures under the selected set of ground motion records. These figures show that both the cable-cylinder and X cable bracing systems significantly decrease the lateral displacement of the frames. However, almost in all cases, the drift ratio is lower in the X cable bracing system compared to the moment-resisting frame and cable-cylinder bracing system. The results indicate that using the cable-cylinder bracing system prevents the damage accumulation in a particular story; it distributes the drifts in frame height. This can be seen in Fig. 3.23. Therefore it can be concluded that strengthening moment-resisting frames by the cable-cylinder system improves their seismic performance due to the approximate distribution of damage in the height of the structure.

3.7 Proposed fiber element modeling technique and validation

As an alternative simulation methodology, in this part, the fiber modeling technique [32] is employed to simulate the nonlinear structural behavior of the cable-cylinder bracing system. The main advantage of the fiber technique is its capability in performing accurate nonlinear analyses in a considerably shorter time comparing to microscopic finite element models.

OpenSees [33] is employed in this study to develop the fiber element model of the steel frame with the cable-cylinder bracing system. A force-based beam-column element is used to simulate the nonlinear behavior of column and beam. The nonlinear behavior of the steel is modeled using *Steel 02* material model available in the OpenSees. To this aim, the postyield hardening ratio is considered to be 1%.

Cable elements are modeled using the Corotational truss element with no compression elastic—perfectly plastic material. InitStressMaterial (available in OpenSees) is used to define the prestressing force in the cables. In the fiber modeling technique, a local coordinate system is assigned for each element that is different from the global system. Various characteristics of each element such as ductility and stiffness should be transformed using the predefined transformation

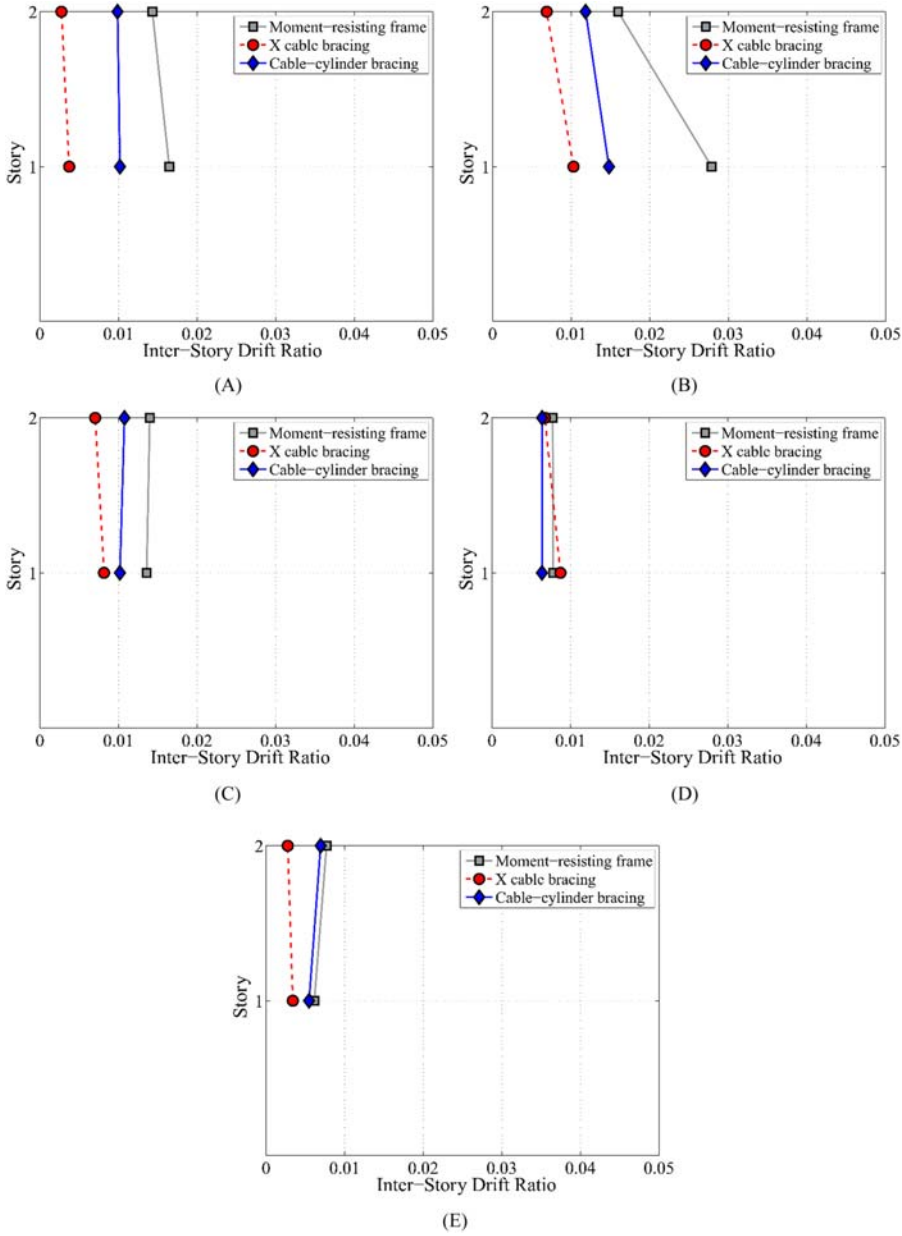

Figure 3.21 Distribution of drift ratios along with the height of 2-story case-study frames under selected ground motions: (A) Bam, (B) Kobe, (C) Loma Prieta, (D) Morgan Hill, and (E) Northridge.

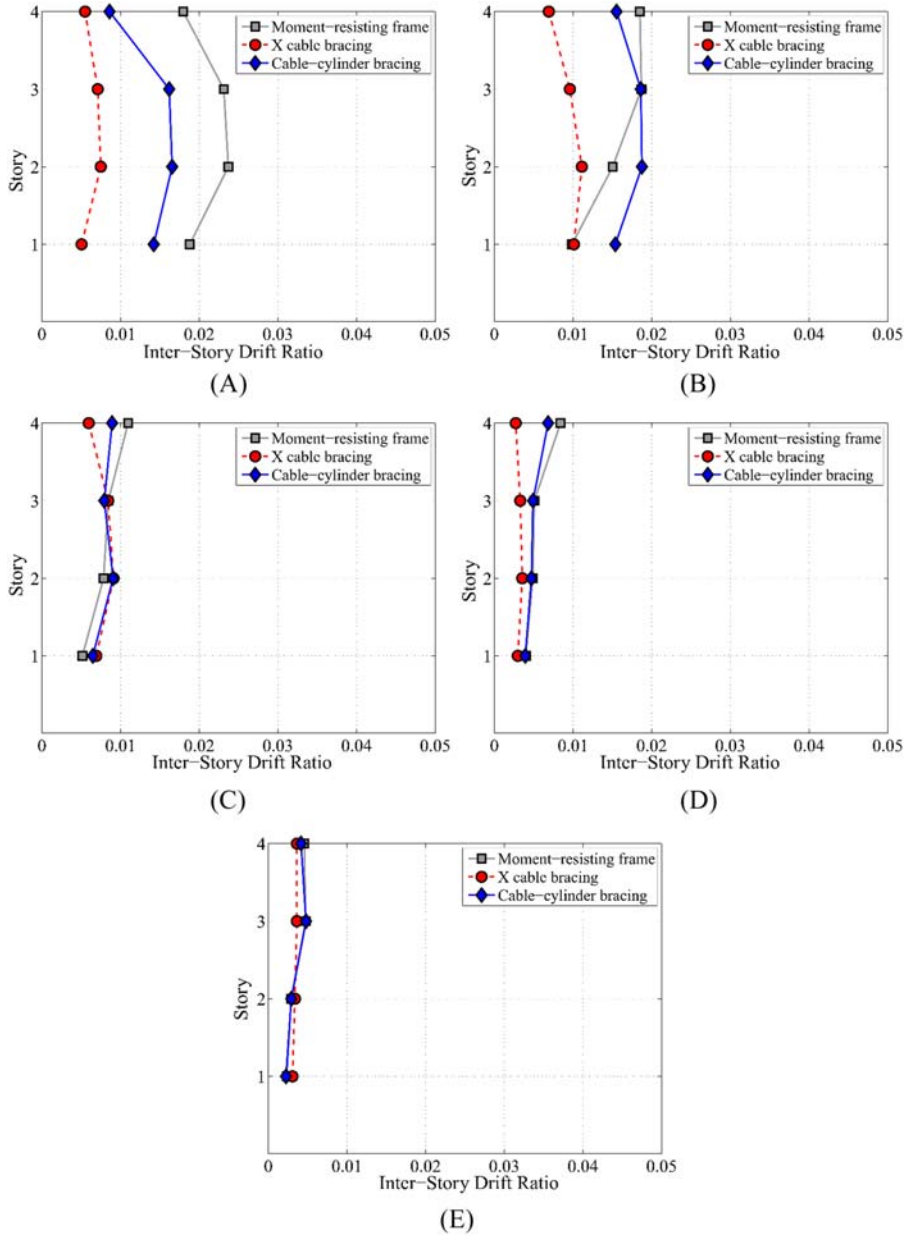

Figure 3.22 Distribution of drift ratios along with the height of 4-storey case-study frames under selected ground motions: (A) Bam, (B) Kobe, (C) Loma Prieta, (D) Morgan Hill, and (E) Northridge.

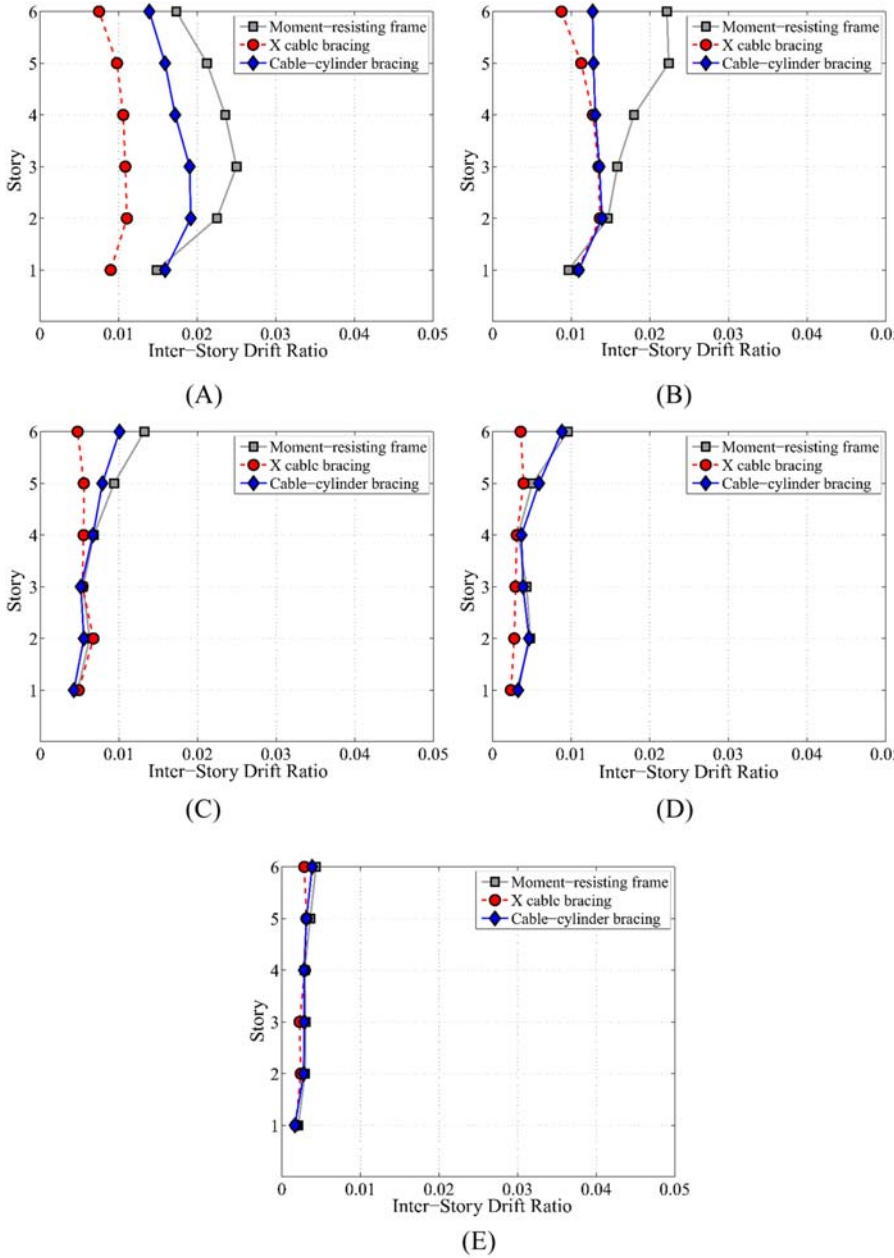

Figure 3.23 Distribution of drift ratios along with the height of 6-storey case-study frames under selected ground motions: (A) Bam, (B) Kobe, (C) Loma Prieta, (D) Morgan Hill, and (E) Northridge.

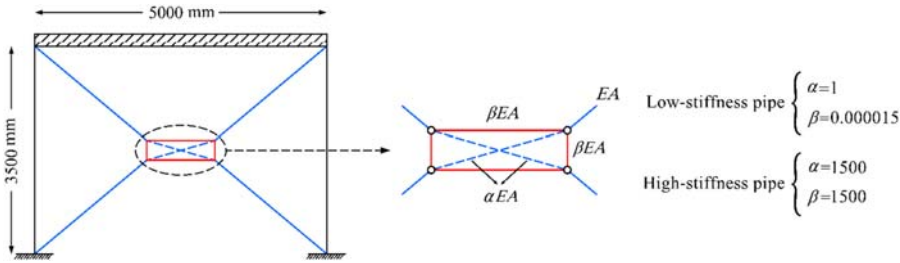

Figure 3.24 Modeling cable and cylinder [26].

Table 3.2 Structural details of cable-cylinder bracing system used in Re. [26].

Modulus of elasticity (MPa)	Cross-sectional area (mm^2)	Rupture strain	Diameter (mm)	Internal diameter (mm)	Cylinder length (mm)
137000	374	0.015	28	200	703

schemes in OpenSees. Here, P-delta transformation is used to consider the secondary effects (P-delta effects) in the nonlinear behaviour of the structural system.

To validate the proposed modeling technique, the structural details of the 1-story steel frame simulated by Hou and Tagawa [26] is adopted here. The details of this frame are shown in Fig. 3.24. The yield strength and elastic modulus of steel are considered to be 300 MPa and 205 GPa. The story height and span length are considered to be 3.5 and 5 m, respectively. The elements of the cable-cylinder bracing system are simulated employing hinged truss elements. To this aim, the axial rigidity of the cylinder and its inner cables are considered 1500 times outside cables [26]. In Table 3.2 the structural details of the cable-cylinder bracing system used in Refs. [26,34] are presented.

Using the developed model in OpenSees, the calculated fundamental period of the structure is 0.69 seconds which shows a good agreement with the one reported in Ref. [26]. In Fig. 3.25 the result of the nonlinear pushover analysis of the proposed model is compared with the result of the pushover analysis conducted by Hou and Tagwa [26]. As can be seen in Fig. 3.25, the proposed modeling technique accurately simulates the base shear−roof displacement response of the considered structure.

Using the outputs of the pushover analysis, the variations of the lateral stiffness of the cable-cylinder bracing system is plotted in Fig. 3.26 against the lateral displacement of the frame. This figure shows that the lateral stiffness of the cable-cylinder bracing system is not a constant parameter; its value depends on the extent of the lateral displacement of the roof.

In Fig. 3.27, the pushover result of the 1-story steel frame braced with the cable-cylinder bracing system is compared with that of the X cable bracing system. To

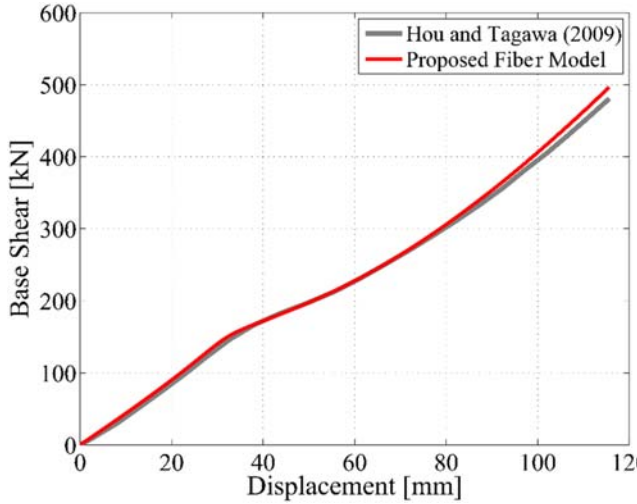

Figure 3.25 Validation of the proposed fiber element modeling technique.

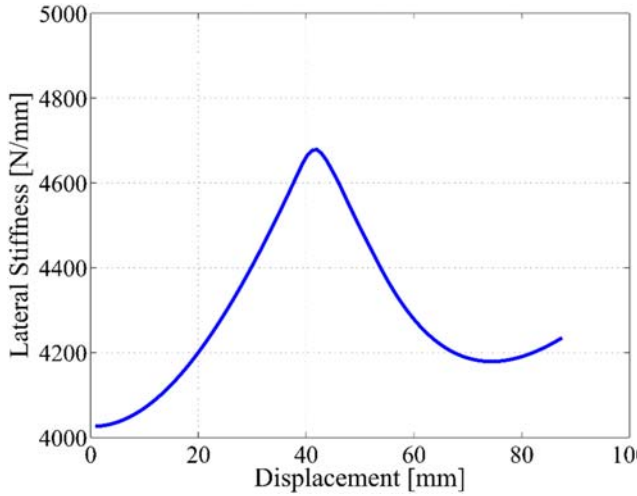

Figure 3.26 Lateral stiffness variation of the cable-cylinder bracing system.

conduct pushover analysis, the target displacement is considered to be $0.02h$, where h is the story height [29]. As can be seen in this figure, the lateral stiffness of the X cable bracing system is significantly greater than the cable-cylinder bracing system. Therefore, this system tolerates higher lateral loading for a given roof displacement. In Table 3.3 the values of base shear associated with the first yielding of the structure are tabulated for both frames. These quantities will be used in Section 3.9 for the calculation of the response modification factor.

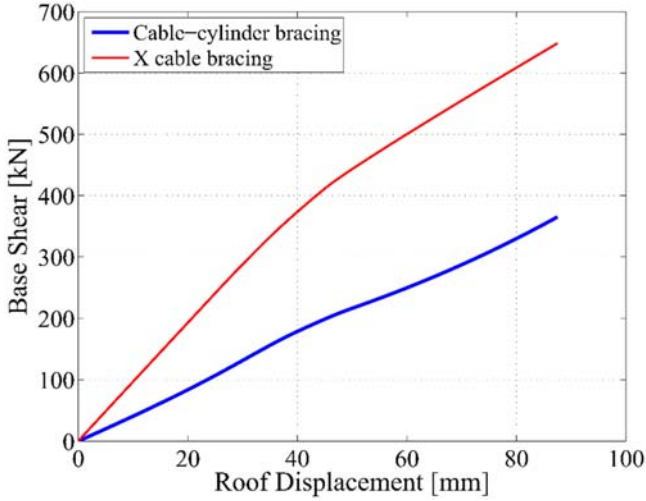

Figure 3.27 Comparing nonlinear pushover analysis results of the cable-cylinder bracing system with the X cable bracing system.

Table 3.3 Base shear associated with the first yielding of the structure.

Structure	Base shear (kN)
Moment-resisting frame braced with the X cable bracing system	361.64
Moment-resisting frame braced with the cable-cylinder bracing system	155.89

3.8 Nonlinear dynamic analysis

The validated model of the 1-story steel frame is adopted in this section to conduct IDA. The first step to carry out IDA is the selection of an appropriate suite of earthquake ground motion records. To conduct IDAs, 10 earthquake records are selected from the far-field ground motion suite presented in FEMA P695 [35]. Details of the selected earthquake records are tabulated in Table 3.4. The PGA of the selected ground motions varies from 0.33 to 0.52 g. Further details are available in Ref. [35].The spectral acceleration at the fundamental period of the structure, Sa(T_1, 5%), is considered here as the intensity measure (IM) and the maximum interstory drift ratio (MIDR) is considered as damage measure. These ground motions are applied to the case-study structure with increasing levels of IMs to cover its response from the elastic response all the way to its complete collapse.

Fig. 3.28 shows the IDA results of the examined frame. As this figure shows, the response of the frame in the elastic range (here up to approximately 0.01 drift ratio) is the same under all the considered ground motions records. However, beyond the elastic range, the response of the frame under each record becomes different from

Table 3.4 Details of the selected ground motion records.

Record no.	Record	Station name	PGA(g)	Occurrence year
1	Chi Chi-Taiwan	CHY101	0.398	1999
2	Hectormine	Hector	0.328	1999
3	Imperial valley	Delta	0.35	1979
4	Kobe	Nishi-Akashi	0.483	1995
5	Landers	Cool Water	0.417	1992
6	Kocaeli	Duzce	0.364	1999
7	Loma Prieta	Capitola	0.511	1989
8	Manjil	Abbar	0.515	1990
9	Northridge	Canyon Country	0.472	1994
10	Superstition Hills	Poe Road	0.475	1987

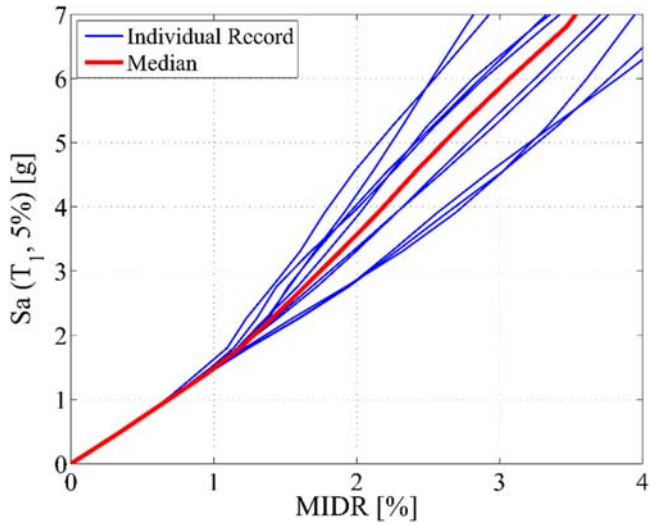

Figure 3.28 IDA results for the 1-storey steel frame braced with the cable-cylinder bracing system. *IDA*, Incremental dynamic analysis.

others, highlighting the importance of considering uncertainties associated with the input excitation. These results will be used in the next section of the study to compute the *R* factor of the frame.

3.9 Response modification factor

In this section, the response modification factor of the considered frame braced with the cable-cylinder bracing system is computed and compared with the conventional X cable bracing system. To this end, nonlinear pushover analysis, IDA, and

linear time-history analyses were conducted on the considered 1-story frame. Using the analyses results, overstrength, ductility and response modification factor of the frame is calculated using the methodology presented in [9] under each ground motion record. It is worth mentioning that, employing FEMA P695 [35] methodology, seismic design coefficients of dual system with cable-cylinder bracing and intermediate moment resisting frame (IMRF) are calculated by Ghasemi et al. [36]. Tables 3.5–3.6 present the obtained results for the frame braced with the X cable bracing system and the cable-cylinder braced frame, respectively. In these tables, DM is the damage limit state of the target performance level of the structure. Here, DM is assumed to be 0.02, corresponding to the limit state of Life Safety (LS) performance level. This assumption was based on the maximum relative story drift ratio threshold proposed in the Standard No. 2800 [31].

$V_{b\ (Dyn,u)}$ is the associated base shear with the DM for each ground motion, which is obtained from the results of the IDA (Fig. 3.28). $V_{b\ (st,y)}$ is the base shear associated with the first yielding of the structure, which is obtained from the results of the pushover analysis (as presented in Table 3.3). $V_{b\ (Dyn,e)}$ is the base shear corresponding to the DM = 0.02 in the linear time-history analysis. It should be noted that to conduct linear time-history analysis, the material behavior of the steel is assumed to be linear. $R_s = V_{b\ (Dyn,u)}/V_{b\ (st,y)}$ and $R_u = V_{b\ (Dyn,e)}/V_{b\ (Dyn,u)}$ are the overstrength factor and ductility factor, respectively. R_{LRFD} and R_{ASD} are response modification factors for the Load and Resistance Factor Design (LRFD) and Allowable Stress Design (ASD) methods, respectively. The average of the results is summarized in Table 3.7. Results tabulated in Tables 3.5–3.7 show that the ductility factor of the cable-cylinder bracing system is greater than that of the X cable bracing system. This is because in the cable-cylinder bracing system cables reach their fracture strain in higher lateral displacement of the roof.

According to the summarized results in Table 3.7, R_{ASD} is 4.94 and 4.17 for the cable-cylinder bracing and X cable bracing systems. This indicates that the response modification factor of the cable-cylinder bracing system is higher than the X cable bracing system. The reason, as discussed earlier in the text, is related to the higher ductility of the cable-cylinder bracing system compared to conventional X cable bracing.

3.10 Influence of structural details on response modification factor

In this section, the influence of cross-sectional details of columns and beams on the response modification factor of the case-study structures is investigated. In Table 3.8, different cross-sectional details of the considered structures as well as the obtained overstrength, ductility, and response modification factors are presented.

Results show that the obtained response modification factors for the weaker beam sections are greater. This is because the first plastic hinge is formed in a relatively lower base shear for the weaker beam section cases, and therefore, the

Table 3.5 Ductility, overstrength, and *R* factors of the frame braced with the X cable bracing system.

Records	**DM** **Max Drift**	**IM** **$S_a(T_1,5\%)$**	$V_{b(Dyn,u)}$ **(kN)**	$V_{b(st,y)}$ **(kN)**	$V_{b(Dyn,e)}$ **(kN)**	R_s	R_μ	R_{LRFD}	R_{ASD}
Chi Chi	0.02	0.62	804.28	361.64	1026.90	2.22	1.28	2.84	4.09
Hectormine	0.02	0.59	801.45	361.64	906.91	2.22	1.13	2.51	3.61
Imperial valley	0.02	0.92	805.24	361.64	1106.06	2.23	1.37	3.06	4.40
Kobe	0.02	0.79	806.43	361.64	1106.43	2.23	1.37	3.06	4.41
Landers (Cool Water)	0.02	0.52	800.97	361.64	960.29	2.21	1.20	2.66	3.82
Kocaeli (Duzce)	0.02	0.59	802.37	361.64	987.95	2.22	1.23	2.73	3.93
Loma Prieta	0.02	0.99	806.96	361.64	1264.75	2.23	1.57	3.50	5.04
Manjil	0.02	2.08	803.35	361.64	1048.47	2.22	1.31	2.90	4.17
Northridge	0.02	1.13	802.05	361.64	937.66	2.22	1.17	2.59	3.73
Superstition	0.02	0.71	806.58	361.64	1118.99	2.23	1.39	3.09	4.46
average	–					2.22	1.30	2.89	4.17
sigma	–					0.12	0.40	0.28	0.30
C.V.	–					0.06	0.31	0.10	0.07

Table 3.6 Ductility, overstrength, and R factors of the frame braced with the cable-cylinder bracing system.

Records	**DM** **Max Drift**	**IM** **$S_a(T_1,5\%)$**	$V_{b(Dyn,u)}$ **(kN)**	$V_{b(st,y)}$ **(kN)**	$V_{b(Dyn,e)}$ **(kN)**	R_s	R_μ	R_{LRFD}	R_{ASD}
Chi Chi	0.02	0.83	372.50	155.89	444.72	2.39	1.19	2.85	4.11
Hectormine	0.02	0.98	353.87	155.89	482.18	2.27	1.36	3.09	4.45
Imperial valley	0.02	0.73	355.03	155.89	469.13	2.28	1.32	3.01	4.33
Kobe	0.02	1.34	360.59	155.89	574.23	2.31	1.59	3.68	5.30
Landers (Cool Water)	0.02	1.25	359.37	155.89	462.35	2.31	1.29	2.97	4.27
Kocaeli (Duzce)	0.02	1.11	359.37	155.89	538.13	2.31	1.50	3.45	4.97
Loma Prieta	0.02	1.81	363.86	155.89	762.98	2.33	2.10	4.89	7.05
Manjil	0.02	1.15	367.38	155.89	654.11	2.36	1.78	4.20	6.04
Northridge	0.02	1.25	368.66	155.89	460.66	2.36	1.25	2.96	4.26
Superstition	0.02	0.73	368.41	155.89	494.89	2.36	1.34	3.17	4.57
average	–		–			2.33	1.47	3.43	4.94
sigma	–		–			0.04	0.27	0.63	0.90
C.V.	–		–			0.02	0.18	0.18	0.18

Table 3.7 The summarized results for overstrength, ductility, and response modification factors.

Structure	R_S	R_μ	R_{LRFD}	R_{ASD}
Moment-resisting frame braced with the X cable bracing system	2.22	1.3	2.89	4.17
Moment-resisting frame braced with the cable-cylinder bracing system	2.33	1.47	3.43	4.94

overstrength factor increases. Moreover, the response modification factor for a given beam section is lower for the lower columns cross-section. This is because the frame with the weaker column section meets the damage limit state in lower base shear values. Furthermore, Table 3.8 shows that, for a given beam section, the base shear associated with forming the first plastic hinge is approximately constant for the frames braced with the cable-cylinder bracing system.

3.11 Sensitivity analysis

In Sections 3.3 and 3.4, it was shown that the cylinder dimensions and prestressing force play a critical role in the seismic performance of the cable-cylinder bracing system. Therefore, in this section, a sensitivity analysis is conducted to study the significance of various parameters, such as u, prestress of cables (f_{ps}) and v to in structural response of cable-cylinder braced frames. As presented in Table 3.9, totally 27 different combinations of u, v, and f_{ps} have been considered for sensitivity analysis.

For each combination tabulated in Table 3.9, IDA is conducted and subsequently, for each case, the response modification response is computed. As an example, in Figs. 3.29 and 3.30 the IDA results are presented for combinations 7 and 27, respectively.

In Tables 3.10 and 3.11, the response modification factor of the one-story frame braced with cable-cylinder braces are tabulated for combination 7 and combination 27, respectively. Table 3.12 presents the mean value of calculated ductility over strength and response modification factors for each combination.

As can be seen in Table 3.12, for all the combinations, the response modification factor of the system decreases as the prestressing force of cables increases. The reason is that when the prestressing force increases, the base shear associated with forming the first plastic hinge increases. Moreover, the fundamental period of the system is reduced with an increase in pre-stress value, leading to a stiffer system.

In most of the considered combinations, an increase in u and a decrease in v increase the ductility factor. This is because, in such cases, the length of cables increases in comparison with their original length. This causes the cable to reach its ultimate strength in the higher drifts. Moreover, the overstrength factor is decreased with an increase in δ_{sr} value.

Table 3.8 Response modification factor for different structural details.

	Beam	**Column**	$V_{b(st,y)}$ **(kN)**	$V_{b(Dyn,u)}$ **(kN)**	$V_{b(Dyn,e)}$ **(kN)**	R_s	R_μ	R_{LRFD}
Moment-resisting frame braced with X cable bracing system	IPE270	IPB200	361.64	803.97	1046.44	2.22	1.3	2.89
	IPE240		282.34	777.10	893.25	2.75	1.15	3.16
	IPE220		218.96	761.92	874.89	3.48	1.15	4.00
	IPE220	IPB200	218.96	761.92	874.89	3.48	1.15	4.00
		IPB180	247.87	735.41	865.86	2.97	1.18	3.49
		IPB160	307.94	711.90	848.08	2.31	1.19	2.75
Moment-resisting frame braced with cable-cylinder bracing system	IPE270	IPB200	155.89	368.66	460.66	2.36	1.25	2.95
	IPE240		106.89	348.57	469.14	3.26	1.35	4.39
	IPE220		73.04	335.63	467.51	4.60	1.39	6.40
	IPE220	IPB200	73.04	335.63	467.51	4.60	1.39	6.40
		IPB180	73.46	306.18	393.07	4.17	1.28	5.35
		IPB160	81.86	282.44	341.92	3.45	1.21	4.18

Table 3.9 Different combinations of cylinder length, prestress of cables, and the inner diameter of the cylinder.

Combination No.	***u***	***v***	f_{ps}	**Combination No.**	***u***	***v***	f_{ps}	**Combination No.**	***u***	***v***	f_{ps}
	(mm)	(mm)	(MPa)		(mm)	(mm)	(MPa)		(mm)	(mm)	(MPa)
1	580	80	100	10	640	80	100	19	700	80	100
2	580	80	300	11	640	80	300	20	700	80	300
3	580	80	500	12	640	80	500	21	700	80	500
4	580	140	100	13	640	140	100	22	700	140	100
5	580	140	300	14	640	140	300	23	700	140	300
6	580	140	500	15	640	140	500	24	700	140	500
7	580	200	100	16	640	200	100	25	700	200	100
8	580	200	300	17	640	200	300	26	700	200	300
9	580	200	500	18	640	200	500	27	700	200	500

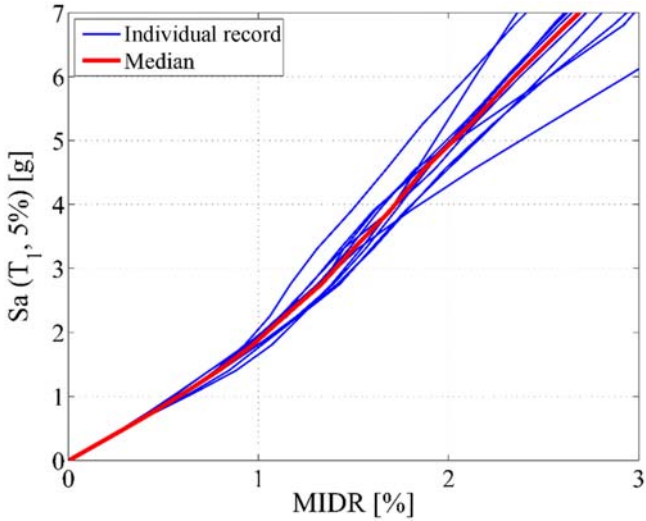

Figure 3.29 IDA results of one-story frame braced with the cable-cylinder bracing system for combination No.7. *IDA*, Incremental dynamic analysis.

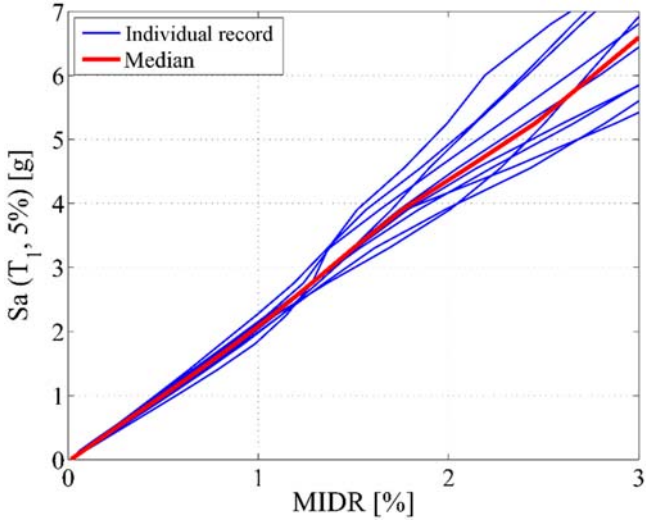

Figure 3.30 IDA results of one-story frame braced with the cable-cylinder bracing system for combination No.27. *IDA*, Incremental dynamic analysis.

However, the decrease in the overstrength factor is greater than the increase in the ductility factor. Therefore, for these combinations, the response modification factor decreases. However, it should be noted that, based on the obtained results, it is hard to make a general conclusion on the relationship between the prestressing force and

Table 3.10 Ductility, overstrength, and *R* factors for combination No. 7.

Records	**DM** **Max drift**	**IM** $S_a(T_1,5\%)$	$V_{b(Dyn,u)}$ **(kN)**	$V_{b(st,y)}$ **(kN)**	$V_{b(Dyn,e)}$ **(kN)**	R_s	R_μ	R_{LRFD}	R_{ASD}
Chi Chi	0.02	0.81	596.52	213.92	694.44	2.79	1.16	3.25	4.67
Hectormine	0.02	0.83	535.53	213.92	625.01	2.50	1.17	2.92	4.21
Imperial valley	0.02	0.68	596.52	213.92	756.28	2.79	1.27	3.54	5.09
Kobe	0.02	1.29	596.52	213.92	796.91	2.79	1.34	3.73	5.36
Landers (Cool Water)	0.02	0.92	516.74	213.92	596.52	2.42	1.15	2.79	4.02
Kocaeli (Duzce)	0.02	1.34	516.74	213.92	619.78	2.42	1.20	2.90	4.17
Loma Prieta	0.02	2.00	516.74	213.92	769.24	2.42	1.49	3.60	5.18
Manjil	0.02	1.14	516.74	213.92	867.08	2.42	1.68	4.05	5.84
Northridge	0.02	1.02	539.47	213.92	815.79	2.52	1.51	3.81	5.49
Superstition	0.02	0.84	534.07	213.92	596.52	2.50	1.12	2.79	4.02
average	–	–				2.55	1.31	3.34	4.80
sigma	–	–				0.16	0.18	0.44	0.64
C.V.	–	–				0.06	0.14	0.13	0.13

Table 3.11 Ductility, overstrength, and *R* factors for combination No. 27.

Records	**DM** **Max drift**	**IM** **$S_a(T_1,5\%)$**	$V_{b(Dyn,u)}$ **(kN)**	$V_{b(st,y)}$ **(kN)**	$V_{b(Dyn,e)}$ **(kN)**	R_s	R_μ	R_{LRFD}	R_{ASD}
Chi Chi	0.02	0.65	475.15	239.49	546.74	1.98	1.15	2.28	3.29
Hectormine	0.02	0.63	475.07	239.49	529.61	1.98	1.11	2.21	3.18
Imperial valley	0.02	0.68	447.94	239.49	730.96	1.87	1.63	3.05	4.40
Kobe	0.02	1.48	459.13	239.49	785.02	1.92	1.71	3.28	4.72
Landers (Cool Water)	0.02	0.82	467.98	239.49	578.66	1.95	1.24	2.42	3.48
Kocaeli (Duzce)	0.02	0.99	452.53	239.49	515.37	1.89	1.14	2.15	3.10
Loma Prieta	0.02	1.52	449.86	239.49	589.09	1.88	1.31	2.46	3.54
Manjil	0.02	1.23	451.59	239.49	713.58	1.89	1.58	2.98	4.29
Northridge	0.02	1.21	476.64	239.49	706.54	1.99	1.48	2.95	4.25
Superstition	0.02	0.58	470.38	239.49	495.83	1.96	1.05	2.07	2.98
average	–	–				1.93	1.34	2.59	3.72
sigma	–	–				0.05	0.23	0.41	0.60
C.V.	–	–				0.02	0.17	0.16	0.16

Table 3.12 The mean value of ductility, overstrength, and *R* factors for considered combinations.

Run	u (mm)	v (mm)	f_{ps} (MPa)	R_s	R_μ	R_{LRFD}
1	580	80	100	1.83	1.68	3.05
2	580	80	300	1.79	1.58	2.83
3	580	80	500	1.77	1.50	2.64
4	580	140	100	2.18	1.46	3.18
5	580	140	300	2.05	1.43	2.92
6	580	140	500	1.92	1.34	2.56
7	580	200	100	2.56	1.31	3.34
8	580	200	300	2.23	1.43	3.20
9	580	200	500	2.04	1.37	2.80
10	640	80	100	1.72	1.72	2.95
11	640	80	300	1.70	1.64	2.78
12	640	80	500	1.70	1.54	2.61
13	640	140	100	2.01	1.56	3.12
14	640	140	300	1.94	1.46	2.83
15	640	140	500	1.84	1.43	2.63
16	640	200	100	2.37	1.41	3.33
17	640	200	300	2.12	1.35	2.85
18	640	200	500	2.02	1.41	2.86
19	700	80	100	1.68	1.73	2.90
20	700	80	300	1.64	1.70	2.77
21	700	80	500	1.64	1.63	2.68
22	700	140	100	1.87	1.65	3.07
23	700	140	300	1.83	1.53	2.81
24	700	140	500	1.80	1.48	2.66
25	700	200	100	2.20	1.45	3.19
26	700	200	300	2.07	1.42	2.92
27	700	200	500	1.93	1.34	2.59

the value of the response modification factor. From Table 3.12, it can be concluded that the *R* factor is more sensitive to the value of the prestressing force of cables, comparing to the other parameters. The sensitivity of the response modification factor versus each considered variables parameter is plotted in Fig. 3.31. As Fig. 3.31 shows, for a constant value of u, the R_{LRFD} is increased significantly with an increase in v. For example, for $u = 600$ mm, the value of *R* factor is obtained at approximately 3, 3.15, and 3.32 for $v = 80$, 140, and 200 mm, respectively.

Fig. 3.32 shows the variation of the response modification factor for a given value of cylinder length. Fig. 3.32 shows that for a given value of cylinder length (here $u = 580$ mm), while the higher v results in a higher *R* factor, increasing the extent of prestressing causes the reduction of the *R* factor.

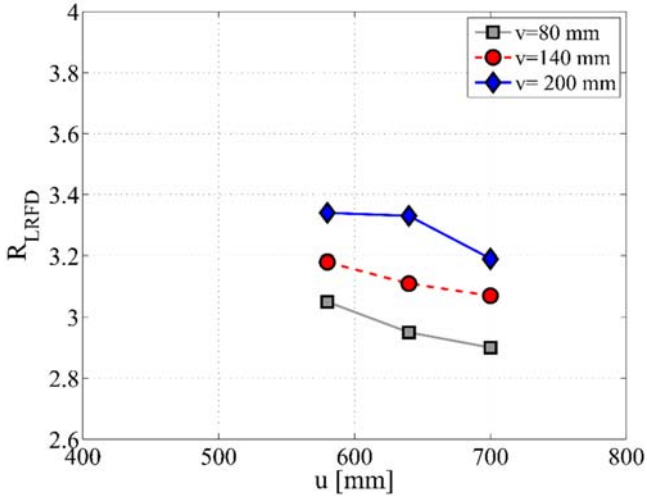

Figure 3.31 The variation of response modification factor against cylinder length and cylinder internal diameter for $f_{ps} = 100$ MPa.

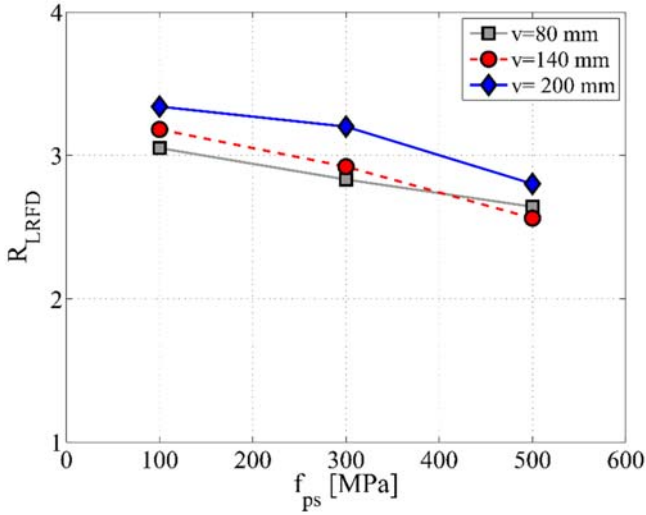

Figure 3.32 The variation of response modification factor against internal cylinder diameter and prestressing for $u = 580$ mm.

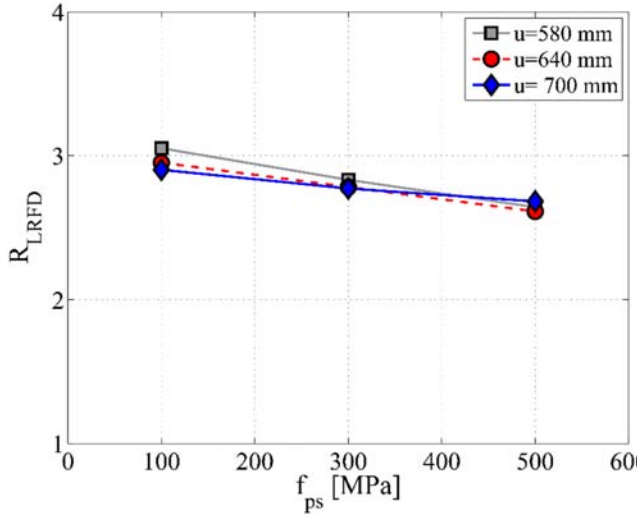

Figure 3.33 The variation of response modification factor against prestressing and cylinder length for $v = 80$ mm.

Table 3.13 The variation of response modification factor against cylinder length and diameter for $f_{ps} = 100$ MPa.

f_{ps} = 100 MPa		
u(mm)	v(mm)	R_{LRFD}
580	80	3.05
580	140	3.18
580	200	3.34
640	80	2.95
640	140	3.11
640	200	3.33
700	80	2.90
700	140	3.07
700	200	3.19

Fig. 3.33 shows the variation of the R factor versus the different cylinder lengths and prestressing force for $v = 80$ mm. As can be seen in this figure, up to about $f_{ps} = 300$ MPa, increasing the cylinder length decreases the R factor. However, for

Table 3.14 The variation of response modification factor against prestressing and cylinder diameter for $u = 580$ mm.

$u = 580$ mm		
v(mm)	f_{ps}(MPa)	R_{LRFD}
80	100	3.05
80	300	2.83
80	500	2.64
140	100	3.18
140	300	2.92
140	500	2.56
200	100	3.34
200	300	3.20
200	500	2.80

Table 3.15 The variation of response modification factor against prestressing and cylinder length for $v = 80$ mm.

v = 80 mm		
u(mm)	f_{ps}(MPa)	R_{LRFD}
580	100	3.05
580	300	2.83
580	500	2.64
640	100	2.95
640	300	2.78
640	500	2.61
700	100	2.90
700	300	2.77
700	500	2.68

higher prestress values increasing the cylinder length leads to a slight increase in the R factor.

The detailed results on variation of response modification factor for different cylinder lengths, prestressing stress of cables, and the internal diameter of the cylinder are tabulated in Tables 3.13−3.15.

3.12 Proposing an equation for the response modification factor of cable-cylinder bracing system

Using the results of sensitivity analysis carried out in the previous section, here an equation is proposed for the response modification factor of the cable-cylinder bracing system in terms of prestress of cables cylinder internal diameter and cylinder length.

Response surface methodology (RSM) describes a relationship between a dependent variable and several independent variables. This methodology is a combination of mathematical and statistical techniques that are used to link the considered response surface (y) and independent input variables (x_1, x_2,..., x_k). Among the existing RSMs, central composite methodology (CCM) is recognized as the most suitable methodology. In this methodology, three different surfaces such as high surface, medium surface, and low surface are assumed for each factor. Each of these surfaces can be used in all the possible experiments (3^k experiments) or a subset of 3^k experiments, where k is the number of the existing independent variables. In the current study, the CCM has been used for developing an equation for the response modification factor [37].

Using the CCM, three different values are assumed for each variable: (1) cylinder lengths to be 580, 640, and 700 mm; (2) cylinder diameters to be 80, 140, and 200 mm, and (3) cables' prestressing level of 100, 300, and 500 MPa. It worth mentioning that Minitab software is used to develop the equations of response modification factor. Eq. (3.26) presents the proposed equation for R_{LRFD} in terms of the considered variables:

$$R_{LRFD} = 7.03 - 0.01297u + 0.00892v - 0.001881f_{ps} + 0.000010u^2 - 0.000003v^2 + 0.000001f^2{}_{ps} - 0.000008uv + 0.000001uf_{ps} - 0.000005vf_{ps} \tag{3.26}$$

To evaluate the accuracy of the proposed Eq. (3.26), the obtained values of R_{LRFD} from Eq. (3.26) are compared with the corresponding calculated response modification factors (as presented in Tables 3.13–3.15) in Table 3.16. As can be seen in Table 3.16, there is a negligible difference between the calculated value of the R factor using the proposed equation and those obtained from the nonlinear analyses. Therefore it can be concluded that Eq. (3.26) is a promising simple way to estimate the R factor of the cable-cylinder bracing system with different cylinder length, prestressing, and cylinder diameter of cables.

Table 3.16 The values of the *R* factor obtained from the incremental dynamic analysis methodology and Minitab software.

No.	u (mm)	v (mm)	f_{ps} (MPa)	R_{LRFD} (calculated)	R_{LRFD} (Minitab)	Error (%)
1	580	80	100	3.05	3.03	0.64
2	580	80	300	2.83	2.77	1.90
3	580	80	500	2.64	2.59	1.74
4	580	140	100	3.18	3.22	1.47
5	580	140	300	2.92	2.90	0.46
6	580	140	500	2.56	2.66	3.84
7	580	200	100	3.34	3.39	1.51
8	580	200	300	3.20	3.01	5.88
9	580	200	500	2.80	2.71	3.32
10	640	80	100	2.95	2.96	0.10
11	640	80	300	2.78	2.71	2.60
12	640	80	500	2.61	2.54	2.70
13	640	140	100	3.11	3.11	0.14
14	640	140	300	2.83	2.81	0.77
15	640	140	500	2.63	2.58	1.94
16	640	200	100	3.33	3.25	2.37
17	640	200	300	2.85	2.88	1.15
18	640	200	500	2.86	2.75	3.74
19	700	80	100	2.90	2.95	1.77
20	700	80	300	2.77	2.71	1.88
21	700	80	500	2.68	2.56	4.59
22	700	140	100	3.07	3.08	0.45
23	700	140	300	2.81	2.78	0.83
24	700	140	500	2.66	2.57	3.52
25	700	200	100	3.19	3.19	0.22
26	700	200	300	2.92	2.83	3.03
27	700	200	500	2.59	2.55	1.18

3.13 Conclusion

In this chapter, concepts of a novel bracing system called cable-cylinder bracing system are introduced. First, the theoretical equilibrium relationships of this system are derivated. Then, the influence of different parameters such as cylinder length, cylinder diameter, cylinder rigidity, and prestressing force on the structural behavior of moment-resisting framer braced with the cable-cylinder bracing system is investigated. Subsequently, the developed theoretical relationships are verified using the finite element model of the proposed bracing system. This is followed then by NTHA of this bracing system. For comparison purposes, in all the analyses, the

structural behavior of the cable-cylinder bracing system is compared with the conventional X cable bracing system. The hysteretic response, drifts distribution, and height of the considered case study frames are discussed. Then, using the fiber element modeling technique, the response modification factor of the proposed bracing system is calculated employing an IDA approach. Finally, a sensitivity analysis is carried out considering various cylinder lengths, cylinder diameters, and prestressing forces. Using the sensitivity analysis outputs, a relationship is introduced for the response modification factor of the steel frames with the cable-cylinder bracing system.

Overall, the research carried out in this chapter confirms that the cable-cylinder bracing system could be a promising alternative for strengthening existing moment-resisting steel frames compared to the conventional X cable bracing system. However, the authors of this chapter believe that further experimental studies with different structural details are required to ensure the adequate seismic performance of this bracing system under large impulsive earthquakes.

References

[1] M. Bruneau, T. Bhagwagar, Seismic retrofit of flexible steel frames using thin infill panels, Engineering Structures 24 (4) (2002) 443−453. Available from: https://doi.org/10.1016/S0141-0296(01)00111-0.

[2] F. Bartera, R. Giacchetti, Steel dissipating braces for upgrading existing building frames, Journal of Constructional Steel Research 60 (3−5) (2004) 751−769. Available from: https://doi.org/10.1016/S0143-974X(03)00141-X.

[3] L.D. Sarno, Bracing systems for seismic retrofitting of steel frames. In: Proceedings of the fifth international conference on behaviour of steel structures in seismic areas, 2006, pp. 821−826.

[4] R.H. Hanson, Supplemental damping for improved seismic performance, Earthquake Spectra 9 (3) (1993) 319−334. Available from: https://doi.org/10.1193/1.1585719.

[5] T.T. Soong, G.F. Dargush, Passive Energy Dissipation Systems in Structural Engineering, John Wiley & Sons, 1997.

[6] I.D. Aiken, D.K. Nims, A.S. Whittaker, J.M. Kelly, Testing of passive energy dissipation systems, Earthquake Spectra 9 (3) (1993) 335−370. Available from: https://doi.org/10.1193/1.1585720.

[7] S. Stefano, G. Terenzi, The damped cable system for seismic protection of frame structures—Part II: design and application, Earthquake Engineering and Structural Dynamics 41 (2012) 929−947. Available from: https://doi.org/10.1002/eqe.1165.

[8] M. Kurata, R. Leon, R. DesRoches, Rapid seismic rehabilitation strategy: concept and testing of cable bracing with couples resisting damper, Journal of Structural Engineering 138 (3) (2012). Available from: https://doi.org/10.1061/(ASCE)ST.1943-541X.0000401.

[9] N. Fanaie, E. Afsar Dizaj, Response modification factor of the frames braced with reduced yielding segment BRB, Structural Engineering and Mechanics 50 (1) (2014) 1−17. Available from: https://doi.org/10.12989/sem.2014.50.1.001.

[10] E. Afsar Dizaj, N. Fanaie, A. Zarifpour, Probabilistic seismic demand assessment of steel frames braced with reduced yielding segment buckling restrained braces,

Advances in Structural Engineering 21 (7) (2018) 1002−1020. Available from: https://doi.org/10.1177/1369433217737115.
[11] M.A. Saleem, M.M. Saleem, Cable Bracing System to Resist Wind Forces on Tall Building in Miami, 3rd FIB International Congress, Washington, DC, USA, 2010.
[12] H. Osamu, S. Kouhei, M. Taro, The role of cables in large span spatial structures: introduction of recent space structures with cables in Japan, Engineering Structures 21 (8) (1999) 795−804. Available from: https://doi.org/10.1016/S0141-0296(98)00029-7.
[13] O. Ben Mekki, F. Auricchio, Performance evaluation of shape-memory-alloy superelastic behavior to control a stay cable in cable-stayed bridges, International Journal of Non-Linear Mechanics 46 (2) (2011) 470−477. Available from: https://doi.org/10.1016/j.ijnonlinmec.2010.12.002.
[14] V. Straupe, A. Paeglitis, Analysis of geometrical and mechanical properties of cable-stayed bridge, Modern Building Materials, Structures and Techniques 57 (2013) 1086−1093. Available from: https://doi.org/10.1016/j.proeng.2013.04.137.
[15] H. Wu, XiangY, J. Wang, Condition assessment of long span cable-stayed bridge, Journal of Zhejiang University SCIENCE A 7 (2) (2006) 297−308. Available from: https://doi.org/10.1631/jzus.2006.AS0297.
[16] H. Kang, Y. Zhao, H. Zhu, Analytical and experimental dynamic behavior of a new type of cable-arch bridge, Journal of Constructional Steel Research 101 (2014) 385−394. Available from: https://doi.org/10.1016/j.jcsr.2014.06.005.
[17] S. Tan and A. Astaneh-Asl, Use of steel cables to prevent progressive collapse of existing buildings. Proceedings of sixth conference on tall buildings in seismic regions, Los Angeles, California, 2003.
[18] M. Hadi, A.T. Saeed, New building scheme to resist progressive collapse, Journal of Architectural Engineering 18 (4) (2012) 324−331. Available from: https://doi.org/10.1061/(ASCE)AE.1943-5568.0000088.
[19] J. Cai, Y. Xu, L. Zhuang, J. Feng, J. Zhang, Comparison of various procedures for progressive collapse analysis of cable-stayed bridges, Journal of Zhejiang University SCIENCE A 13 (5) (2012) 323−334. Available from: https://doi.org/10.1631/jzus.A1100296.
[20] M. Razavi, M.R. Sheidaii, Seismic performance of cable zipper-braced frames, Journal of Constructional Steel Research 74 (2012) 49−57. Available from: https://doi.org/10.1016/j.jcsr.2012.02.007.
[21] M. Kurata, R. Leon, R. DesRoches, Rapid seismic rehabilitation strategy: concept and testing of cable bracing with couples resisting damper, Journal of Structural Engineering 138 (3) (2012). Available from: https://doi.org/10.1061/(ASCE)ST.1943-541X.0000401.
[22] S. Chuang, Y. Zhuge, P.C. McBean, Seismic retrofitting of unreinforced masonry walls by cable system, 13th World Conference on Earthquake Engineering, Vancouver, Canada, 2004.
[23] S.M. Zahrai, M.J. Hamidia, Studying the Rehabilitation of Existing Structures Using Compound System of Cables and Shape Memory Alloys. ATC & SEI Conference on Improving the Seismic Performance of Existing Buildings and Other Structures, San Francisco, California, 2009.
[24] H. Tagawa, X. Hou, Seismic retrofit of ductile moment resisting frames using wire-rope bracing, Proceedings of the eighth pacific conference on earthquake engineering, 2007.
[25] N. Fanaie S. Aghajani, S. Shamloo Theoretical assessment of wire rope bracing system with soft central cylinder. 15th World Conference on Earthquake Engineering, Lisbon, Portugal, 2012.

[26] X. Hou, H. Tagawa, Displacement-restraint bracing for seismic retrofit of steel moment frames, Journal of Constructional Steel Research 65 (5) (2009) 1069−1104. Available from: https://doi.org/10.1016/j.jcsr.2008.11.008.
[27] N. Fanaie, S. Aghajani, E. Afsar Dizaj, Strengthening of moment-resisting frame using cable-cylinder bracing, Advances in Structural Engineering 19 (11) (2016) 1736−1754. Available from: https://doi.org/10.1177/1369433216649382.
[28] American Institute of Steel Construction (AISC), ANSI/AISC360−10: Specification for Structural Steel Buildings, AISC, Chicago, IL, 2010.
[29] American Society of Civil Engineers (ASCE), Minimum design loads for buildings and other structures (ASCE7-10), ASCE, Reston, VA, 2010.
[30] PEER (Pacific Earthquake Engineering Research Center). PEER NGA ground motion database. http://peer.berkeley.edu/nga; 2011.
[31] Standard No 2800 V4. Iranian code of practice for seismic resistant design of buildings. Tehran, Iran: Building and Housing Research Center, 2014.
[32] F. Taucer, E. Spacone, F.C. Filippou, A fiber beam-column element for seismic response analysis of reinforced concrete structures. Berkeley: EERC College of Engineering, University of California, 1991.
[33] F. McKenna, OpenSees: a framework for earthquake engineering simulation, Computing in Science and Engineering 13 (4) (2011) 58−66. Available from: https://doi.org/10.1109/MCSE.2011.66.
[34] G.D. Nolan, Bond properties of CFCC Prestressing strand in pretensioned concrete beams. Master of Science in Civil Engineering, Department of Civil and Geological Engineering, University of Manitoba, 1995.
[35] FEMA P695, Quantification of building seismic performance factors. Federal Emergency Management Agency, Washington, DC, 2009.
[36] M. Ghasemi, N. Fanaie, H. Khorshidi, Seismic performance factors of a dual system with IMRF and cable-cylinder bracing, Journal of Building Engineering (2021). Available from: https://doi.org/10.1016/j.jobe.2021.102309 (in press).
[37] A. Khuri, s Mukhopadhyay, Response surface methodology, Wiley Interdisciplinary Reviews: Computational Statistics 2 (2) (2010) 128−149.